Technical Report 2

NASA-JPL (5926-9)
Contract No. 950875

Jet Propulsion Laboratory

California Institute of Technology

Pasadena, California

Stress-Strain Behavior of an Inert Composite Propellant for Multiaxial Loading Conditions

by

M. G. Sharma and Y. S. Lee

The Pennsylvania State University
Department of Engineering Mechanics
University Park, Pennsylvania

August 1965

RE-ORDER NO. 65-627

Technical Report 2

NASA-JPL (5926-9)
Contract No. 950875
under NAS 7-100

Jet Propulsion Laboratory

California Institute of Technology

Pasadena, California

Stress-Strain Behavior of an Inert Composite Propellant for Multiaxial Loading Conditions

by

M. G. Sharma and Y. S. Lee

The Pennsylvania State University
Department of Engineering Mechanics
University Park, Pennsylvania

August 1965

Table of Contents

Preface

This report is the second of a series of technical reports on research work conducted under research project entitled "A Test Program to Determine the Mechanical Behavior of Solid Fuel Propellants". The work reported here particularly refers to mechanical characterization of an inert composite propellant for biaxial loading conditions from its observed behavior under uniaxial tension loading. The effect of rate of loading on stress-strain behavior is considered. The report includes experimental data on the behavior of the material under several biaxial stress fields, for two rates of loading. The experimental data has been compared with predicted values based on linear viscoelastic theory and finite viscoelastic theory.

Stress-Strain Behavior of an Inert Composite Propellant under Multiaxial Loading Conditions

by

M. G. Sharma and Y. S. Lee

I. Introduction

Mechanical characterization of solid fuel propellants has gained importance in recent years due to its need in the stress-strain analysis of propellant grains subjected to complex loading and environmental conditions in some of the present day rocket systems. Most solid fuel propellants under normal temperatures display large deformation and viscoelastic effects when subjected to external loading. The linear viscoelastic theory [1]* which describes time dependent response of any material fairly accurately is not strictly suitable for a propellant material undergoing large time dependent deformation. On the other hand finite elastic theory that considers the large deformation behavior cannot be applied to propellant materials without modification to include time effects. Although, some continuum theories [2] that include both time dependent and finite deformation characteristics are available, very little work has been done to experimentally verify whether such theories describe adequately the mechanical behavior of solid fuel propellants. In an earlier investigation [3] attempts have been made to characterize inert composite propellants displaying both viscoelastic and large deformation effects, in terms of a stored energy function and a dissipated energy function. Even though the above investigation has given some insight into the behavior of the material under multiaxial loading conditions, the interpretation has been complicated by the scatter in data

*Numbers in brackets refer to bibliography.

due to variations in mechanical behavior of the material molded into specimens under identical conditions and lack of experimental arrangement that could impose precise load history. In the present investigations great care is taken to eliminate the inconsistencies of the earlier program by standardizing specimen preparation method and by developing a new biaxial loading device [4] that could impose precise load histories.

II. Experimental Investigations

(a) Material and specimen preparation.

The material used in this investigation is a composite dummy propellant that is a copolymer of Butadiene and Acrylic acid crosslinked with Epon 828. Finely divided aluminum of particle size 10 micron is used as a filler agent in the preparation of the material.

The proportion of various constituents in the dummy propellant is the following:

(1)	Hycar 2000 x 131, B. F. Goodrich Chemical Co.,	24.4%
(2)	Epon 828, Shell Development	5.7%
(3)	H-10 Aluminum, Valley Aluminum	69.9%

The procedure for the preparation of the dummy propellant as recommended by the Allegany Ballistics Laboratory, Cumberland, Maryland is described as follows.

The ingredients are added in a container in the order given above and treated for half an hour at 180°F. They are mixed thoroughly until the aluminum is completely dispersed. This operation must be done in a properly vented area. To decrease the viscosity the mixture is put into an oven for one-half hour at 180°F. The mixture is evacuated for approximately thirty minutes in a container large enough to allow for an expansion five times its original volume. After evacuation, the mixture is placed in the oven for an additional heating period of fifteen minutes (to decrease viscosity for casting operations). Next the mixture is poured into a preheated mold (180°F) and cured for three days at 180°F.

Preparation of void free specimens was a formidable problem. After considerable effort this was finally solved by preventing entrapping of any air through effective evacuation process. Plans are underway to improve the quality of specimens still further by casting the specimens with the mold maintained under high vacuum. In addition, the removal of the specimens from the mold without damaging them posed a serious problem. This was also solved by application of the proper amount of silicone grease to the inner wall of the mold and the mandrel. Care was taken to remove the cast specimens without any prestressing. A typical tubular specimen used in this investigation is shown in Fig. 1 and a flat specimen used to study uniaxial tension properties is shown in Fig. 2. It was found that the mechanical behavior of the test material depends on post curing period*. In order to obtain consistent experimental data it was very essential to standardize the specimens. The standardization was achieved by conforming to the recipe closely while preparing the specimens and post curing the specimens under constant temperature (75°F) and 50% humidity for a specified number of days (preferably 5 to 6 days). In addition, to insure void free specimens the casting must be done in vacuum.

(b) Mechanical behavior of the test material.

The effect of rate of loading on the uniaxial tension behavior is studied by subjecting tubular specimens to monotonically increasing load at constant loading rates (nominal tension stress rates) and observing the extension in the axial direction. The results are shown in Fig. 3. In the same figure are noted the stress values at fracture corresponding

*The post curing period is defined here as the total time that elapsed between the time of removal of the specimen from the mold and the time of testing. During this period the specimens were maintained at 75°F and 50% humidity environment.

to various rates of loading.

The behavior of the material in creep is studied by subjecting flat specimens (Fig. 2) to constant values of loads and observing elongation in the axial direction of the specimens. The creep data is presented in the form of variation of creep compliance function $D(t)$* with $\log t$ (where t = time) in Fig. 4. As is seen from the figure the creep compliance function varies with stress σ_o, implying the material is slightly non-linear viscoelastic.

However, Fig. 4 shows that the compliance function does not vary with stress in a consistent fashion. Therefore, for computation purposes a mean compliance function is obtained. The mean creep compliance curve is found to obey the following relation.

$$D(t) = D_o + D\,(1 - e^{-\frac{t}{\tau}}) + \frac{t}{\eta} \tag{1}$$

where D_o = initial compliance, $(3.6 \times 10^{-3}\ \text{psi}^{-1})$

D = retarded elasticity, $(4.5 \times 10^{-4}\ \text{psi}^{-1})$

τ = retardation time, (1.09 hrs.)

η = flow viscosity. 6.67×10^{5} (psi-hrs.)

Equation (1) represents a four element Kelvin model (see Fig. 4).

The behavior of the material under isotropic compression (triaxial compression) is found to be viscoelastic. In Fig. 5 is plotted the bulk creep compliance function $B(t)$ obtained from volumetric creep experiments [5] against $\log t$. It was found that the creep behavior corresponded to a three element model (see Fig. 5). The equation for bulk creep compliance function then becomes

$$B(t) = B_o + B\,(1 - e^{-\frac{t}{\lambda}}) \tag{2}$$

*Note: The creep compliance function is the ratio of strain ϵ to stress σ_o in a creep test.

B_o = initial bulk compliance, (21.8×10^{-7} psi^{-1})

B = bulk retarded elastic compliance, (5.28×10^{-7} psi^{-1})

λ = retardation time. (2.5 hrs.)

(c) Apparatus for multiaxial loading.

The apparatus used for studying multiaxial stress-strain behavior is essentially the one described in an earlier technical report on multiaxial fracture studies [4].

(d) Strain measurements.

The deformation of tubular specimens in the multiaxial experiments was evaluated by measuring the axial elongation and the variations in internal and external diameters during tests. These measurements were made through clip gages and in a manner precisely same as described in the earlier report [4].

(e) Experimental program.

The mechanical behavior of the inert composite propellant was studied for a uniaxial and five biaxial stress fields. The stress fields as represented by stress ratios α were 0, 0.32, 0.82, 1.29, 1.68 and 2.29.

$$\left(\text{where } \alpha = \frac{\sigma_{22}'}{\sigma_{11}'} = \frac{\text{nominal principal stress in tangential direction.}}{\text{nominal principal stress in axial direction.}}\right)$$

The behavior under these uniaxial and biaxial stress fields was observed at two rates of loading namely $k = 0.01$ and 10 psi/sec. (where k represents nominal stress rate in the maximum principal stress direction). Three tests were conducted under identical conditions for each of the stress fields mentioned above. This gave an idea of the amount of scatter in the data.

(f) Description of multiaxial stress-strain experiments.

Tubular specimens were subjected to progressively increasing internal pressure. The rate of pressure was held constant during any test.

The stress ratio during any test was determined by the top head used in the biaxial apparatus. Corresponding to any pressure value during the test simultaneous record of internal, external diameters and axial elongations was made. From the value of pressure at any instant, nominal tangential stress and nominal axial stress were calculated. Extension ratios in the tangential, axial and radial directions were calculated from measured values of internal and external diameters and axial elongation.

(g) Experimental results.

In Table 1 are given the data from five biaxial and one uniaxial stress field experiments for two rates of loading. The same data are shown plotted in Figs. 6 to 9. The points shown in Figs. 6 to 9 represent the averages of three or more identical tests.

III Theoretical Considerations

(a) Introduction.

Experimental data (Figs. 6 to 9) indicate that the maximum extension ratio occurs in uniaxial tension and is about 1.32 for the rate of loading of 10 psi/sec. For all the biaxial stress field experiments the maximum extension ratio does not exceed 1.12 (except for stress ratio $\alpha = 0.322$). Although the material displays large deformation in uniaxial tension, there results considerable reduction in deformation under biaxial loading. This suggests that linear viscoelastic theory may well describe the behavior of the material under multiaxial loading. In the following comparison between experimental results and predicted values based upon linear viscoelastic theory and finite elastic theory has been made.

(b) Three dimensional stress-strain relations by linear viscoelastic theory.

The three dimensional stress-strain relations for a isotropic linear viscoelastic material [4] can be shown to be

$$\epsilon_{11} = \left[D(t)\ \sigma_{11} - \left(\frac{D(t)}{2} - \frac{B(t)}{6}\right)(\sigma_{22} + \sigma_{33})\right]$$

$$\epsilon_{22} = \left[D(t)\ \sigma_{22} - \left(\frac{D(t)}{2} - \frac{B(t)}{6}\right)(\sigma_{33} + \sigma_{11})\right] \qquad (3)$$

$$\epsilon_{33} = \left[D(t)\ \sigma_{33} - \left(\frac{D(t)}{2} - \frac{B(t)}{6}\right)(\sigma_{11} + \sigma_{22})\right]$$

where $D(t)$ = creep compliance function in uniaxial tension.

$B(t)$ = creep compliance function in volumetric compression.

$\epsilon_{11}, \epsilon_{22}, \epsilon_{33}$ = principal strains.

$\sigma_{11}, \sigma_{22}, \sigma_{33}$ = principal stresses.

Using equation (3) and the Boltzmann superposition principle it is possible to predict strains for any given stress history. They are:

$$\epsilon_{11} = \left[\int_0^t D(t-t')\frac{d\sigma_{11}}{dt'}\ dt' - \int_0^t \left(\frac{D(t-t')}{2} - \frac{B(t-t')}{6}\right)\frac{d(\sigma_{22} + \sigma_{33})}{dt'}\ dt'\right]$$

$$\epsilon_{22} = \left[\int_0^t D(t-t')\frac{d\sigma_{22}}{dt'}\ dt' - \int_0^t \left(\frac{D(t-t')}{2} - \frac{B(t-t')}{6}\right)\frac{d(\sigma_{11} + \sigma_{33})}{dt'}\ dt'\right]$$

$$\epsilon_{33} = \left[\int_0^t D(t-t')\frac{d\sigma_{33}}{dt'}\ dt' - \int_0^t \left(\frac{D(t-t')}{2} - \frac{B(t-t')}{6}\right)\frac{d(\sigma_{22} + \sigma_{11})}{dt'}\ dt'\right]$$

(4)

where t = present time

t' = past time

For biaxial loading corresponding to

$$\text{stress ratio } \alpha = \frac{\sigma_{22}}{\sigma_{11}}$$

$$\text{stress rate } k = \left(\frac{\sigma_{11}}{t'}\right)$$

equation (4) becomes

$$\epsilon_{11} = \left[\left(1 - \frac{\alpha}{2}\right) k \int_0^t D(t-t')\ dt' + \frac{\alpha k}{6} \int_0^t B(t-t')\ dt'\right]$$

$$\epsilon_{22} = \left[\left(\frac{2\alpha-1}{2}\right) k \int_0^t D(t-t')\ dt' + \frac{k}{6} \int_0^t B(t-t')\ dt'\right] \qquad (5)$$

$$\epsilon_{33} = \left[-(1+\alpha)\ k \int_0^t \left(\frac{D(t-t')}{2} - \frac{B(t-t')}{6}\right) dt'\right]$$

Equation (5) determines the three principal strains for any biaxial stress field (designated by α) and stress rate k, provided the creep properties of the material in uniaxial torsion and volumetric compression are known. Using experimentally determined creep compliance functions (equation 1 and 2) theoretical three dimensional stress-strain relations (equation 5) were evaluated for all the different stress fields (uniaxial and biaxial) and compared with experimental results in Figs. 10 to 14 and table 2.

(c) Mechanical characterization by finite viscoelastic theory.

In the previous section three dimensional stress-strain relations were derived from creep compliance functions in tension and volumetric deformations. These creep compliance functions were obtained by linearizing an otherwise observed nonlinear behavior (see Fig. 4). In this section characterization of the material is made by considering the observed nonlinear behavior. From uniaxial creep data $\sigma'/\left(\lambda - \frac{1}{\lambda^2}\right)$ versus $\frac{1}{\lambda}$ plots at various constant values of time were found to be horizontal straight lines (see Fig. 15). This indicates that uniaxial creep behavior for the material can be adequately described by

$$\sigma' = \left(\lambda - \frac{1}{\lambda^2}\right) C(t) \qquad (6)$$

where σ' = nominal uniaxial tension stress

λ = axial extension ratio

$C(t)$ = creep modulus function

Equation (6) indicates that the material can be characterized for multiaxial loading by the following energy function.

$$W = C(t)\,(I_1 - 3) \tag{7}$$

where W = energy stored in the material at any stage of deformation.

$I_1 = \lambda_1^2 + \lambda_2^2 + \lambda_3^2$ = the first strain invariant

$\lambda_1, \lambda_2, \lambda_3$ principal extension ratios.

In Fig. 16 is shown plotted the variation of creep modulus function with time.

Using equation (7) three dimensional stress-extension ratio relations can be written down as follows [6]

$$\begin{aligned}
\sigma_{11} - \sigma_{33} &= C\ (t)\left[\lambda_1^2 - \lambda_3^2\right] \\
\sigma_{22} - \sigma_{33} &= C\ (t)\left[\lambda_2^2 - \lambda_3^2\right] \\
\sigma_{33} - \sigma_{11} &= C\ (t)\left[\lambda_3^2 - \lambda_1^2\right]
\end{aligned} \tag{8}$$

Equation (8) apply only to a particular stress history--that of creep. Equation (8) can be generalized to be applicable to any stress history by using a modified superposition principle [7]. For biaxial stress conditions ($\sigma_{33} = 0$)the generalized equations become

$$\begin{aligned}
F_1\ (\lambda) &= \int_0^t \frac{1}{C\ (t-t')}\ \frac{d\sigma'_{11}}{dt'}\ dt' \\
F_2\ (\lambda) &= \int_0^t \frac{1}{C\ (t-t')}\ \frac{d\sigma'_{22}}{dt'}\ dt'
\end{aligned} \tag{9}$$

where $$F_1(\lambda) = \left(\lambda_1^2 - \lambda_3^2\right)/\lambda_1$$

$$F_2(\lambda) = \left(\lambda_2^2 - \lambda_3^2\right)/\lambda_2$$

are strain functions.

$\sigma'_{11} = \sigma_{11}/\lambda_1$ and $\sigma_{22}' = \sigma_{22}/\lambda_2$ nominal stresses.

From equation (9) strain functions can be predicted provided the stress histories under biaxial loading are known.

For a biaxial stress history of the following type

$$\sigma_{11}' = kt$$

$$\frac{\sigma_{22}'}{\sigma_{11}'} = \alpha$$

equation (9) reduces to

$$F_1(\lambda) = k \int_0^t \frac{1}{C(t-t')} \, dt' \qquad (10)$$

$$F_2(\lambda) = \alpha k \int_0^t \frac{1}{C(t-t')} \, dt' \qquad (11)$$

Rewriting equations (10) and (11)

$$\frac{d\, F_1(\lambda)}{K dt} = \frac{d\, F_1(\lambda)}{d\, \sigma_{11}'} = \frac{1}{C\ (t)} \qquad (12)$$

and

$$\frac{d\, F_2(\lambda)}{\alpha k\ dt} = \frac{d\, F_2(\lambda)}{d\, \sigma_{22}'} = \frac{1}{C\ (t)} \qquad (13)$$

The validity of equation (12) is checked by plotting strain functions $F_1(\lambda)$ versus nominal axial stress σ_{11}' and determining slopes at various stress values (corresponds to specific time values) for all biaxial stress fields studied experimentally. The measured slopes are compared with the theoretical slopes (inverse of creep modulus function) in Table 3.

IV Discussion of Results.

Although test specimens used in this program were prepared carefully to eliminate any inconsistencies in material behavior due to variations in molding procedure, there seem to be much scatter in the data.

Effect of biaxial stress fields is to reduce the extension ratios in either directions—tangential and axial directions (see Table 1). The mechanical behavior seems to be a border line case where both linear and finite viscoelastic theories may apply. This is to a certain extent substantiated by the predictions based upon the linear viscoelastic theory as is seen from Figs. 10 to 14. In Figs. 10 and 13 for stress ratio of 1.681, axial stress-strain curves predicted and experimentally determined compare reasonably well. The value of maximum strains for these cases is approximately 3%. Figs. 10 and 12 show deviations between experimental and theoretical values are great for uniaxial tension case (stress ratio $\alpha = 0$) for which the strain value is greater than 12%. Table 3 shows the comparison of creep modulus function predicted from the finite visco-elastic theory (Section C) and experimentally obtained from uniaxial creep tests. Although for uniaxial tension case (stress ratio $\alpha = 0$) the deviation between theoretical and experimental values is high, for stress ratios of 0.824 and 1.288 the predictions are reasonably good (see Table 3).

BIBLIOGRAPHY

[1] D. R. Bland, "Linear Viscoelasticity", Pergamon Press, London, 1960.

[2] A. C. Eringen, "Non-Linear Theory of Continous Media", McGraw-Hill Book Company, New York, 1962.

[3] M. G. Sharma and C. K. Lim, "Mechanical Properties of Solid Propellants for Combined States of Stress at Various Temperatures", Final Report to Allegany Ballistics Laboratory, Cumberland, Maryland, Under Subcontract 70NORD 16640.

[4] M. G. Sharma and C. K. Lim, "Failure of an Inert Composite Propellant under Multiaxial Stress Fields", Tech. Report 1, submitted to J.P.L. under Contract No. 950875 in March 1965.

[5] M. G. Sharma and V. D. McCarty, "Experimental Investigations on the Dynamic Compressibilities of Polymeric Materials", A paper presented at the Vth International Symposium on High Speed Testing in Boston, Mass., March, 1965.

[6] L. R. Trelonr, "Physics of Rubber Elasticity", Oxford, 1953.

TABLE 1. Uniaxial and Biaxial Experimental Data for the Inert Composite Propellant.

No. of Test	Stress Ratio $\alpha=\frac{\sigma_{22}}{\sigma_{11}}$	Rate of Loading	Principal Stress: Axial True Stress (psi) σ_{11}	Principal Stress: Tangential True Stress (psi) σ_{22}	Principal Extension Ratio: (Axial) λ_1	Principal Extension Ratio: (Tangential) λ_2	Principal Extension Ratio: (Radial) λ_3
1	0	0.01	11.751	0	1.018	0.992	1.001
			28.664	0	1.058	0.975	0.987
			48.645	0	1.096	0.958	0.971
			61.758	0	1.118	0.947	0.955
			74.452	0	1.132	0.938	0.952
			87.294	0	1.144	0.928	0.952
2	0	0.01	6.407	0	1.012	0.994	1.000
			32.802	0	1.060	0.971	0.978
			67.406	0	1.116	0.943	0.935
			93.993	0	1.132	0.922	0.930
			114.857	0	1.148	0.912	0.905
			118.454	0	1.144	0.905	0.917
3	0	0.01	11.801	0	1.022	0.991	0.999
			17.270	0	1.024	0.988	0.995
			21.032	0	1.032	0.986	0.989
			62.685	0	1.102	0.951	0.967
			80.117	0	1.134	0.938	0.956
			84.403	0	1.138	0.938	0.952
4	0	0.01	6.407	0	1.012	0.994	1.000
			19.354	0	1.056	0.982	0.987
			41.785	0	1.086	0.955	0.958
			64.307	0	1.116	0.930	0.934
			71.327	0	1.132	0.920	0.905
			93.914	0	1.138	0.903	0.909

Uniaxial and Biaxial Experimental Data for the Inert Composite Propellant (continued)

No. of Test	Stress Ratio $\alpha = \frac{\sigma_{22}'}{\sigma_{11}'}$	Rate of Loading psi/sec.	Principal Stress: Axial True Stress (psi) σ_{11}	Principal Stress: Tangential True Stress (psi) σ_{22}	Principal Extension Ratio: (Axial) λ_1	Principal Extension Ratio: (Tangential) λ_2	Principal Extension Ratio: (Radial) λ_3
1	0.824	0.01	6.827	8.612	1.012	1.008	0.979
			12.164	13.984	1.0196	1.012	0.968
			20.730	22.843	1.032	1.019	0.948
			26.963	29.488	1.039	1.025	0.931
			34.279	37.547	1.049	1.034	0.921
			40.954	45.084	1.058	1.041	0.911
			48.384	53.813	1.069	1.050	0.894
			56.427	63.642	1.080	1.060	0.869
2	0.824	0.01	6.812	8.564	1.012	1.006	0.983
			12.841	14.600	1.020	1.010	0.972
			18.445	20.344	1.029	1.015	0.160
			26.011	28.238	1.037	1.021	0.943
			32.471	35.221	1.048	1.027	0.927
			36.259	39.408	1.056	1.031	0.919
			43.274	47.328	1.062	1.039	0.911
			50.512	55.698	1.073	1.046	0.892
3	0.824	0.01	6.80	8.584	1.009	1.008	0.983
			11.407	13.240	1.016	1.012	0.972
			19.608	21.582	1.025	1.017	0.962
			24.413	26.700	1.033	1.022	0.948
			30.300	33.071	1.043	1.028	0.937
			37.891	41.492	1.053	1.036	0.919
			43.851	48.362	1.062	1.043	0.910
			51.496	57.416	1.072	1.052	0.892
4	0.824	0.01	6.858	8.642	1.017	1.007	0.975
			13.006	14.852	1.026	1.012	0.958
			19.209	21.214	1.036	1.017	0.946
			26.298	28.686	1.044	1.023	0.931
			33.479	36.411	1.054	1.029	0.917
			40.939	44.769	1.064	1.037	0.899
			48.576	53.617	1.073	1.045	0.881
			55.781	62.433	1.086	1.055	0.871

Uniaxial and Biaxial Experimental Data for the
Inert Composite Propellant (continued)

No. of Test	Stress Ratio $\alpha=\frac{\sigma_{22}'}{\sigma_{11}'}$	Rate of Loading psi/sec.	Principal Stress: Axial True Stress (psi) σ_{11}	Principal Stress: Tangential True Stress (psi) σ_{22}	Principal Extension Ratio: (Axial) λ_1	Principal Extension Ratio: (Tangential) λ_2	Principal Extension Ratio: (Radial) λ_3
1	1.288	0.01	1.942	6.859	1.001	1.009	0.985
			7.248	15.339	1.004	1.0198	0.979
			23.042	42.754	1.018	1.051	0.931
			27.685	55.125	1.032	1.097	0.879
			51.140	103.5	1.040	1.128	0.838
			54.999	114.81	1.048	1.147	0.833
2	1.288	0.01	0.603	4.716	1.002	1.004	0.998
			25.432	47.828	1.026	1.062	0.906
			32.621	60.491	1.025	1.066	0.908
			39.573	74.931	1.030	1.084	0.890
			48.563	95.109	1.040	1.108	0.861
1	1.682	0.01	2.451	11.092	1.004	1.015	0.980
			5.513	17.649	1.006	1.024	0.971
			36.743	101.830	1.022	1.136	0.837
			42.263	122.428	1.027	1.168	0.817
2	1.682	0.01	12.406	32.698	1.008	1.036	0.954
			23.137	59.178	1.014	1.070	0.919
			35.206	95.060	1.018	1.115	0.769
			32.860	86.223	1.020	1.102	0.881
1	2.289	0.01	5.46	25.789	1.002	1.031	0.963
			13.30	51.645	1.001	1.067	0.926
			16.67	64.340	1.000	1.086	0.904
			22.40	87.614	0.999	1.119	0.872
			25.98	104.856	0.997	1.150	0.881
2	2.289	0.01	0.456	11.081	1.000	1.015	0.981
			7.765	33.318	1.000	1.045	0.945
			17.644	68.006	1.000	1.091	0.902
			21.968	85.899	0.999	1.118	0.879
			24.142	97.807	0.984	1.145	0.862

Uniaxial and Biaxial Experimental Data for the
Inert Composite Propellant (continued)

No. of Test	Stress Ratio, $\alpha = \frac{\sigma_{22}'}{\sigma_{11}'}$	Rate of Loading psi/sec.	Principal Stress: Axial True Stress (psi) σ_{11}	Principal Stress: Tangential True Stress (psi) σ_{22}	Principal Extension Ratio: (Axial) λ_1	Principal Extension Ratio: (Tangential) λ_2	Principal Extension Ratio: (Radial) λ_3
1	0	10	25.083	0	1.036	0.982	0.977
			58.709		1.084	0.959	0.962
			98.052		1.140	0.936	0.937
			138.599		1.196	0.914	0.915
			182.622		1.250	0.893	0.896
			228.749		1.320	0.871	0.858
			273.064		1.440	0.854	0.854
			294.127		1.440	0.847	0.842
2	0	10	24.899	0	1.034	0.983	0.983
			52.670		1.074	0.964	0.962
			84.970		1.122	0.943	0.940
			122.217		1.178	0.922	0.919
			169.200		1.228	0.901	0.900
			214.785		1.290	0.880	0.885
			262.733		1.354	0.860	0.873
			293.838		1.382	0.849	0.862
1	0.322	10	23.054	8.864	1.032	0.992	0.974
			54.127	20.135	1.076	0.985	0.949
			104.315	37.746	1.148	0.974	0.915
			179.285	63.278	1.276	0.964	0.887
			205.025	75.645	1.426	0.985	0.907
2	0.322	10	25.117	9.666	1.036	0.994	0.963
			50.650	18.100	1.076	0.986	0.942
			94.914	34.432	1.148	0.975	0.910
			116.072	41.465	1.208	0.968	0.875
			214.545	79.294	1.408	0.986	0.812
3	0.322	10	24.884	9.546	1.038	0.992	0.974
			50.153	18.704	1.076	0.985	0.952
			82.551	30.189	1.124	0.978	0.933
			148.347	52.784	1.226	0.967	0.883
			220.305	78.848	1.394	0.970	0.828

Uniaxial and Biaxial Experimental Data for the
Inert Composite Propellant (continued)

No. of Test	Stress Ratio $\alpha = \frac{\sigma_{22}}{\sigma_{11}}$	Rate of Loading psi/sec.	Principal Stress: Axial True Stress (psi) σ_{11}	Principal Stress: Tangential True Stress (psi) σ_{22}	Principal Extension Ratio: (Axial) λ_1	Principal Extension Ratio: (Tangential) λ_2	Principal Extension Ratio: (Radial) λ_3
1	0.824	10	7.856	9.635	1.008	1.009	0.981
			25.245	27.624	1.028	1.024	0.942
			48.966	53.968	1.090	1.045	0.894
			72.459	83.557	1.156	1.076	0.844
			96.835	118.673	1.224	1.112	0.790
2	0.824	10	7.490	9.239	1.008	1.007	0.985
			23.482	25.488	1.026	1.017	0.962
			47.160	51.215	1.052	1.037	0.908
			71.148	79.565	1.080	1.059	0.873
			95.384	111.543	1.108	1.087	0.835
3	0.824	10	7.812	9.614	1.004	1.010	0.985
			26.429	28.645	1.026	1.021	0.954
			49.711	54.004	1.052	1.038	0.913
			74.424	83.225	1.080	1.060	0.869
			99.704	116.375	1.108	1.086	0.831
4	0.824	10	7.891	9.668	1.008	1.008	0.977
			26.584	28.943	1.032	1.023	0.946
			49.020	53.909	1.062	1.044	0.894
			73.211	83.276	1.092	1.068	0.850
			105.516	128.800	1.122	1.110	0.738
1	1.288	10	3.697	9.555	1.010	1.010	0.990
			20.301	36.911	1.034	1.034	0.956
			40.113	73.732	1.068	1.068	0.912
			59.825	117.081	1.113	1.113	0.865
			80.128	172.010	1.172	1.172	0.812
2	1.288	10	3.681	9.561	1.013	1.013	0.992
			19.884	36.870	1.043	1.043	9.946
			39.192	74.368	1.085	1.085	0.898
			59.057	120.356	1.136	1.136	0.846
			74.795	168.306	1.199	1.199	0.835

Uniaxial and Biaxial Experimental Data for the
Inert Composite Propellant (continued)

No. of Test	Stress Ratio $\alpha = \frac{\sigma_{22}}{\sigma_{11}}$	Rate of Loading psi/sec.	Principal Stress: Axial True Stress (psi) σ_{11}	Principal Stress: Tangential True Stress (psi) σ_{22}	Principal Extension Ratio: (Axial) λ_1	Principal Extension Ratio: (Tangential) λ_2	Principal Extension Ratio: (Radial) λ_3
1	1.682	10	1.783	9.690	1.000	1.011	0.978
			7.926	22.656	1.002	1.024	0.968
			14.160	36.624	1.006	1.038	0.949
			21.033	53.041	1.009	1.056	0.933
			33.217	86.145	1.018	1.096	0.894
2	1.682	10	1.782	9.635	1.000	1.009	0.981
			7.228	20.999	1.002	1.019	0.974
			13.893	35.693	1.006	1.033	0.949
			21.106	52.325	1.014	1.046	0.923
			35.132	88.278	1.016	1.080	0.885
3	1.682	10	1.783	9.690	1.000	1.011	0.978
			7.297	21.360	1.002	1.023	0.962
			13.652	35.776	1.006	1.040	0.934
			20.718	52.754	1.012	1.059	0.913
			36.384	95.367	1.027	1.104	0.853
1	2.289	10	2.731	17.600	1.001	1.018	0.968
			9.300	37.356	1.001	1.038	0.949
			16.873	63.120	1.003	1.069	0.907
			27.178	100.811	1.004	1.103	0.878
			41.650	166.267	1.008	1.167	0.808
2	2.289	10	9.268	36.727	1.000	1.031	0.958
			16.656	60.285	1.000	1.052	0.934
			25.316	90.912	1.000	1.081	0.907
			34.555	127.316	1.004	1.113	0.872
			44.952	178.891	1.009	1.170	0.827
3	2.289	10	1.974	15.488	1.000	1.018	0.968
			8.374	35.180	1.000	1.046	0.946
			17.525	67.344	1.000	1.088	0.898
			26.644	104.145	1.016	1.129	0.849
			43.432	176.857	1.016	1.206	0.785

TABLE 2. Comparison of Experimental Data with Prediction by Linear Viscoelastic Theory.

Biaxial Stress Ratio $\alpha = \frac{\sigma_{22}'}{\sigma_{11}'}$	Rate of Loading psi/sec.	Axial Stress (psi) Experimental	Axial Stress (psi) Theoretical	Axial Percentage of Deviation %	Tangential Stress (psi) Experimental	Tangential Stress (psi) Theoretical	Tangential Percentage of Deviation %
0	0.01	9 29 43 55 71	6 19 27 35 43	-33.3 -34.5 -37.2 -36.4 -39.5	0	0	0
0.824	0.01	5.0 18.4 32.4 44.6 54.5	4.6 14.0 24.0 33.7 41.9	-8 -22 -26 -24.5 -23	9.8 18.5 26.5 36.5 43.8	6.4 13.9 21.6 32.2 40.5	-34.7 -24.8 -18.5 -11.8 - 7.5
1.288	0.01	12.3 24.5 37.0 46.5 52.2	7.3 16.3 24.2 30.6 35.3	-40.5 -33.5 -34.5 -34 -32.5	12.5 31.6 46.8 61.5 72.5	7.0 22.3 36.2 52.5 68.0	-44 -29.5 -22.7 -14.6 - 6.2
1.682	0.01	5.2 12.7 20.5 31.5 38.6	6.3 14.0 22.0 32.5 40.5	21 10 7 3 5	12.5 35.1 51.9 64.2 71.7	7.0 24.2 41.4 57.0 68.0	-44 -31 -20 -11 - 5
2.289	0.01	Data are not reliable			11.0 23.0 44.5 60.2 71.0	6.0 13.5 29.5 44.0 54.0	-45.5 -42 -33.8 -27 -24

Comparison of Experimental Data with Prediction by
Linear Viscoelastic Theory (continued)

Biaxial Stress Ratio $\alpha = \frac{\sigma_{22}'}{\sigma_{11}'}$	Rate of Loading psi/sec.	Axial Stress (psi) Experimental	Axial Stress (psi) Theoretical	Percentage of Deviation %	Tangential Stress (psi) Experimental	Tangential Stress (psi) Theoretical	Percentage of Deviation %
0	10	61	22	-64	0	0	0
		113	53	-53			
		155	85	-45			
		189	117	-38			
		209	143	-31.5			
0.322	10	53.0	30	-43.5	Date are not reliable		
		97.0	66	-32.0			
		135.0	105	-22.2			
		164.0	140	-14.5			
		182.0	169	- 7.0			
0.824	10	18.0	11	-39	28	20	-28.5
		35.0	22	-37	44	35	-19.5
		51.0	32	-37.3	57	50	-12.3
		65.0	41	-37.0	67	64	- 4.5
		77.0	49	-36.5	72	77	7
1.288	10	11.0	7.0	-36.5	30.0	20	-33.4
		25.7	15.5	-39.2	55	38	-31
		40.0	24.5	-38.8	76	53	-30
		60.5	41.7	-31.0	93	70	-24.7
		74.8	54.0	-27.7	105	90	-14
1.682	10	5.0	3.4	-32	14.5	7.0	-51.7
		13.7	11.0	-19.5	29.7	14.8	-50.2
		21.3	18.5	-13.0	42.2	22.5	-46.4
		27.5	25.5	- 7	52.1	30.8	-41
		32.0	30.5	- 4.5	59.5	39.4	-33.7
2.289	10	Data are not reliable			20	13	-35
					40	28	-30
					60	44	-26.5
					77	60	-22
					90	72	-20

TABLE 3. Comparison of Experimental Data with Prediction by Finite Viscoelastic Theory.

Biaxial Stress Ratio $\alpha = \frac{\sigma_{22}'}{\sigma_{11}'}$	Rate of Loading psi/sec.	Inverse of Creep Modulus Function C(t): Experimental (From Uniaxial creep tests)	Inverse of Creep Modulus Function C(t): Theoretical (By Finite Viscoelastic Theory)	Percentage of Deviation %
0	0.01	0.0082	0.00400	-51.2
		0.00846	0.00450	-46.8
		0.00860	0.00500	-41.9
		0.00870	0.00500	-42.5
		0.00880	0.00500	-43.2
		0.00885	0.00505	-42.9
		0.00892	0.00600	-32.7
0.824	0.01	0.00800	0.00839	4.5
		0.00860	0.00900	4.6
		0.00880	0.00950	8.0
		0.00890	0.00950	6.7
		0.00896	0.0105	17.2
1.288	0.01	0.00820	0.00625	-23.8
		0.00860	0.00770	-10.5
		0.00870	0.00800	- 8.0
		0.00870	0.00850	- 2.3
		0.00890	0.00860	- 3.4
		0.00897	0.00880	- 1.9
1.682	0.01	0.00830	0.00500	-39.8
		0.00880	0.00600	-31.9
		0.00890	0.00600	-32.6
		0.00896	0.00740	-17.4
2.289	0.01	0.00822	0.00567	-31.1
		0.00877	0.00567	-35.4
		0.00887	0.00567	-36.1
		0.00896	0.00778	-13.2
		0.00896	0.00778	-13.2

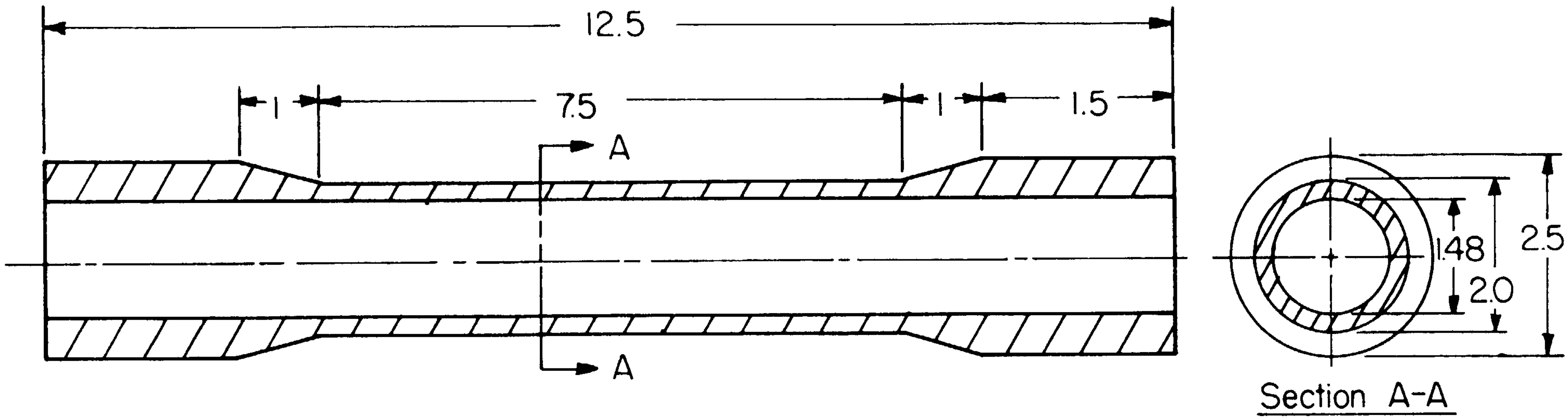

FIG. 1 A TYPICAL TUBULAR SPECIMEN

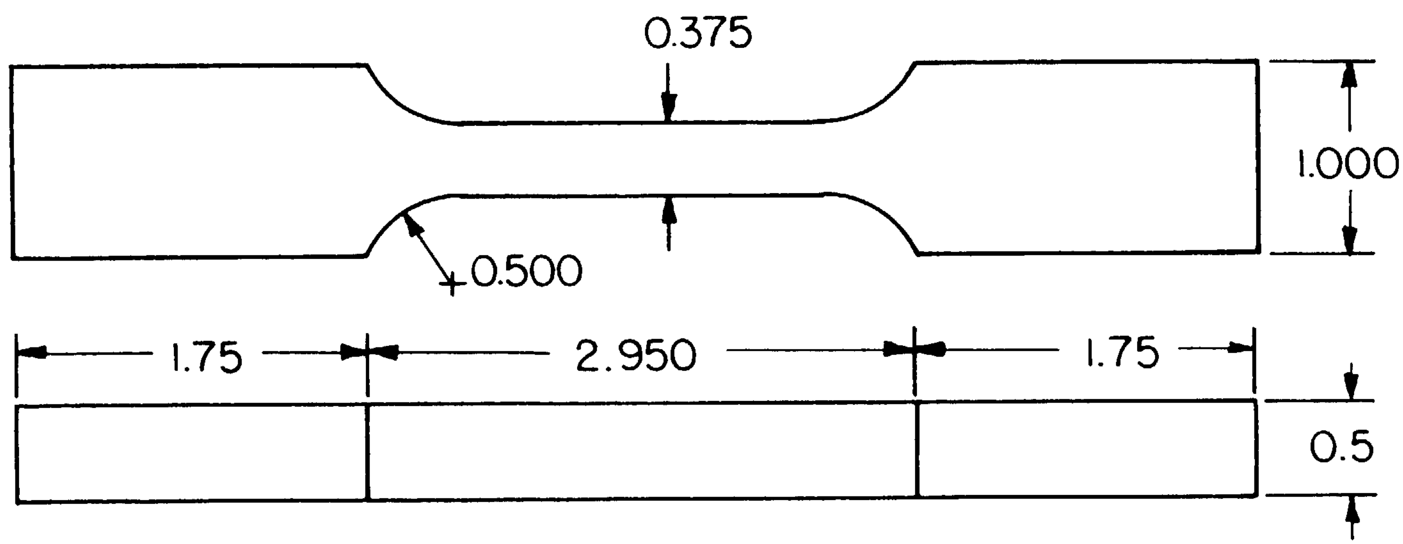

FIG. 2 A TYPICAL FLAT SPECIMEN (JANAF)

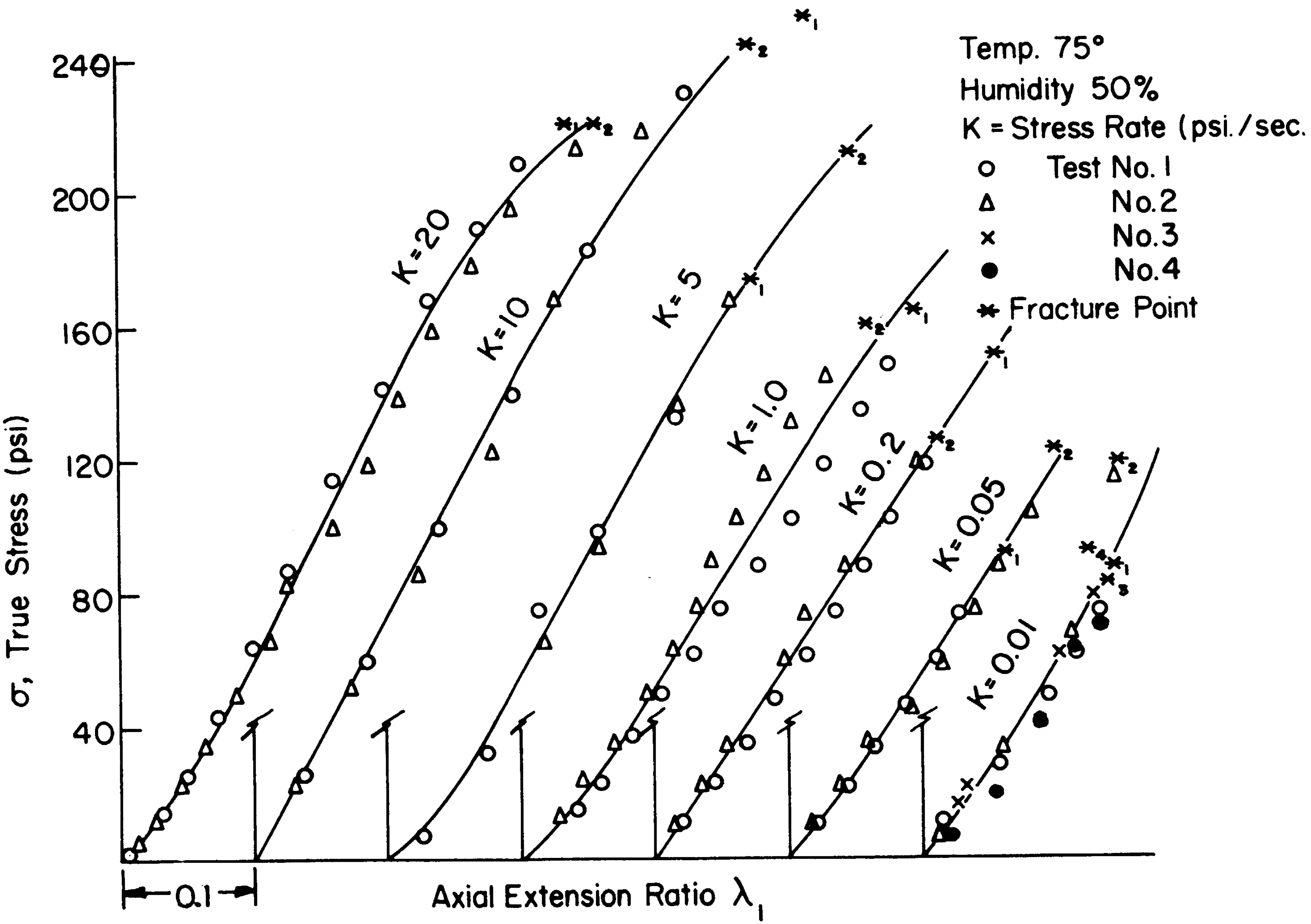

FIG. 3 TRUE STRESS vs AXIAL EXTENSION RATIO FOR THE INERT COMPOSITE PROPELLENT

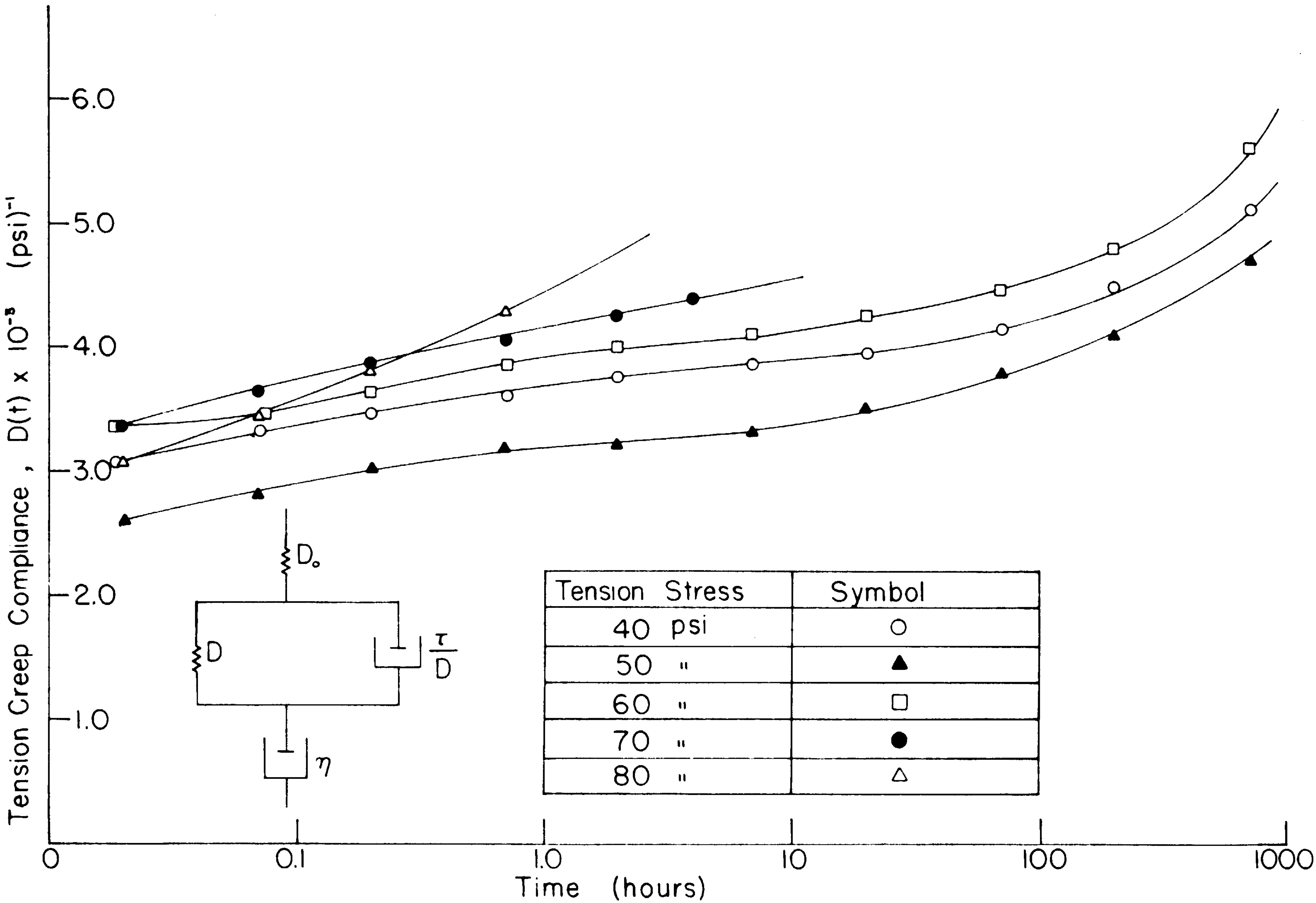

FIG. 4 VARIATION OF TENSION CREEP COMPLIANCE WITH TIME FOR THE INERT COMPOSITE PROPELLANT

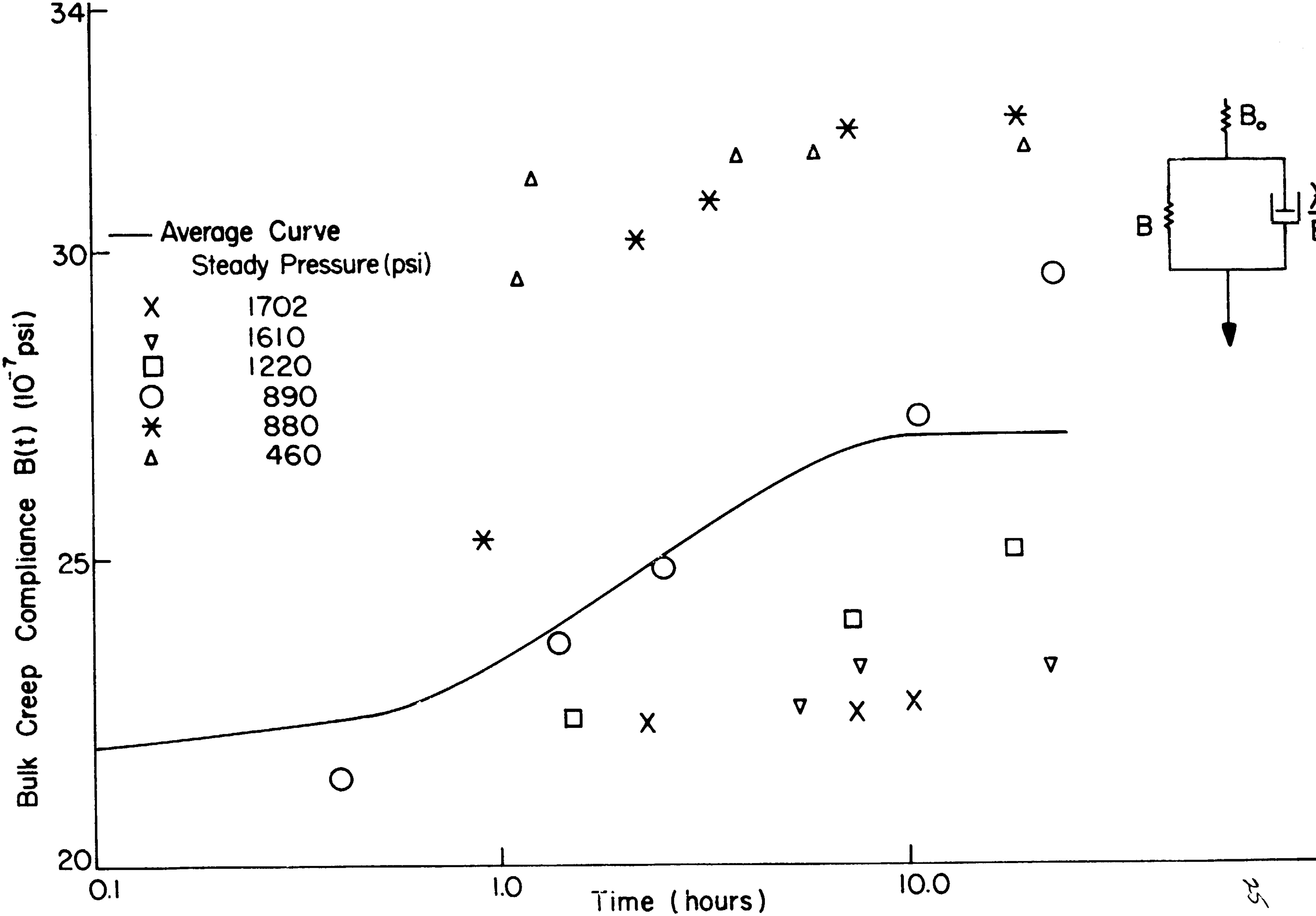

25

FIG. 5 VARIATION OF BULK CREEP COMPLIANCE WITH TIME FOR THE INERT COMPOSITE PROPELLENT

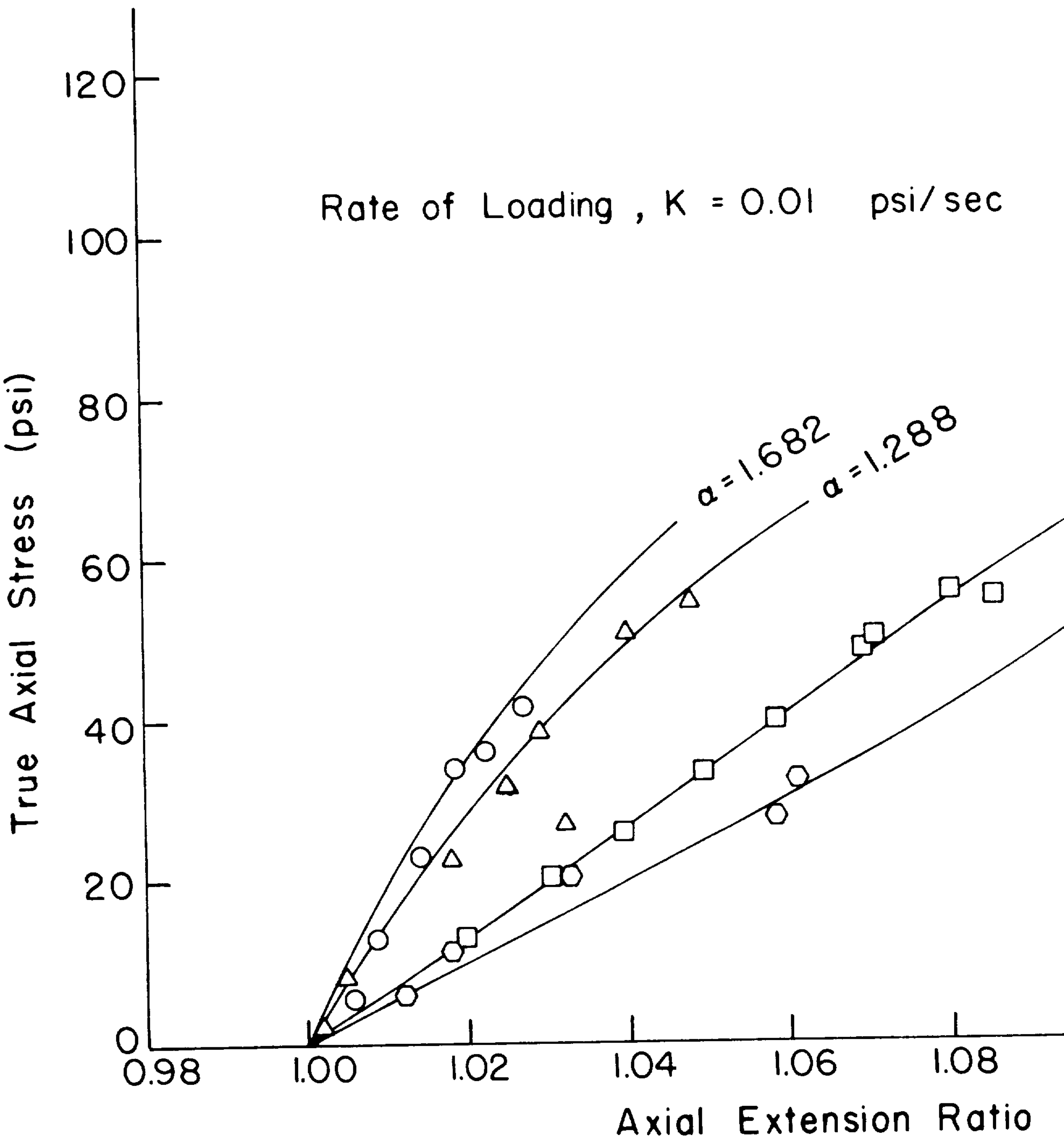

FIG. 6 TRUE AXIAL STRESS — AXIAL EXTENS
PROPEL

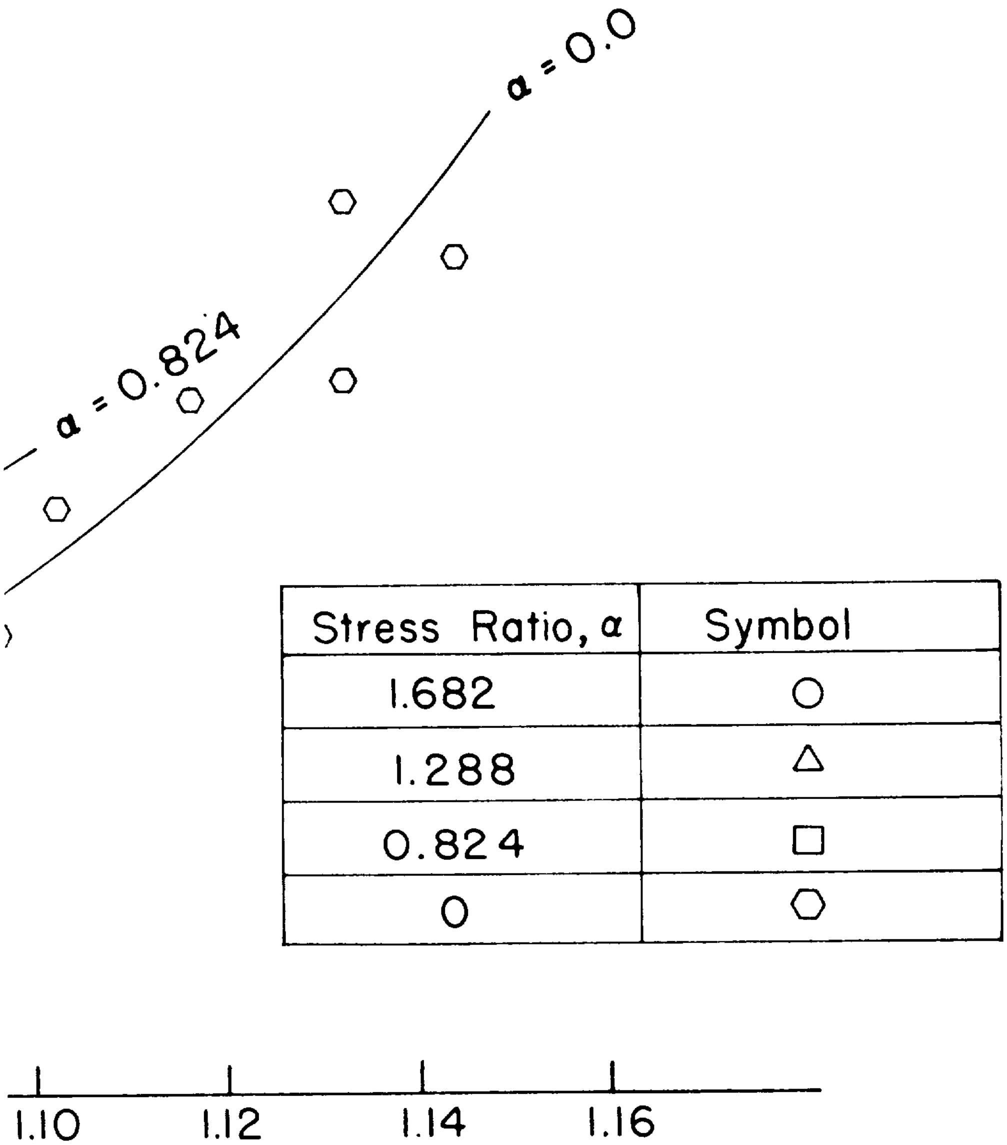

N RATIO CURVES FOR THE INERT COMPOSITE
ANT

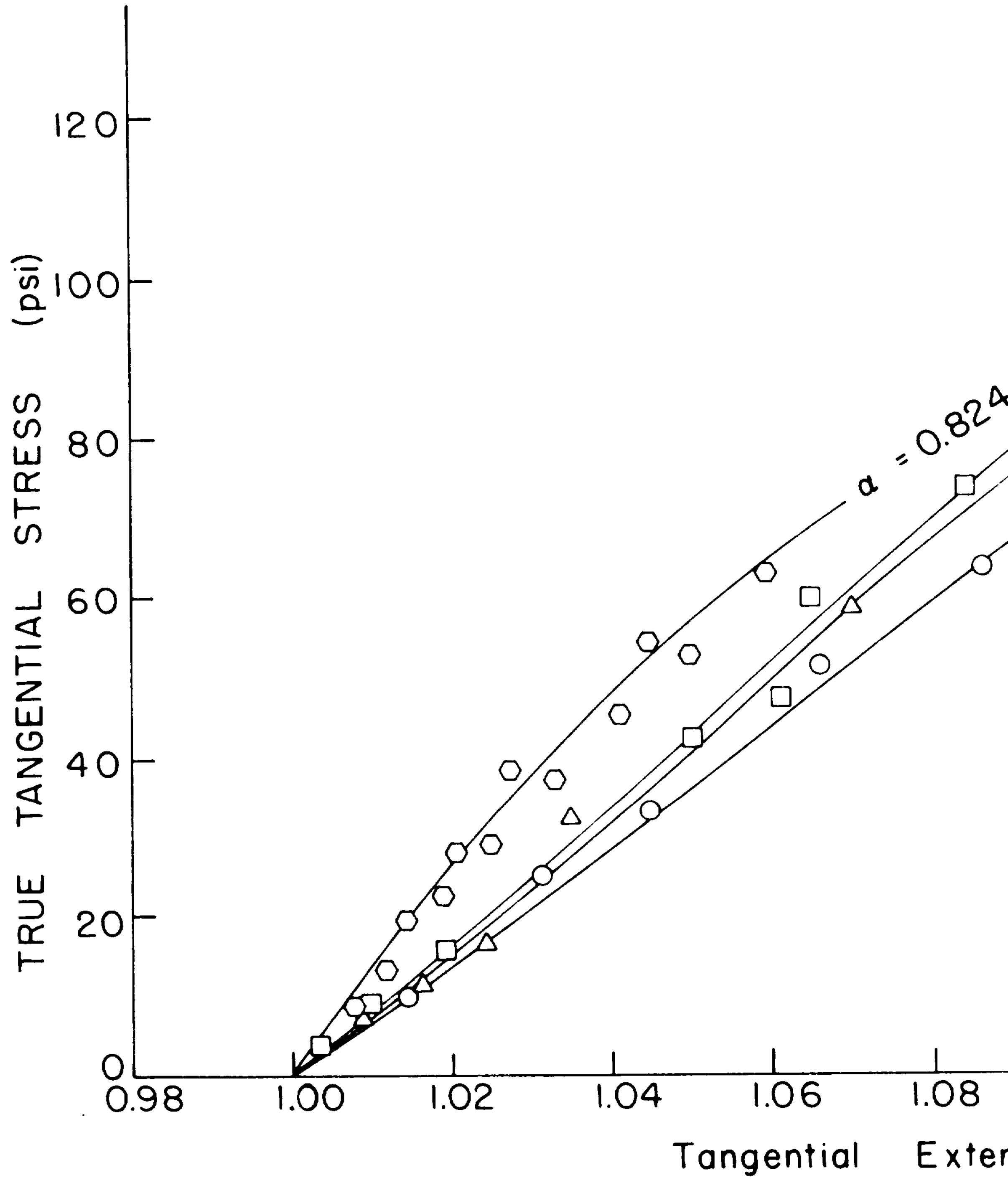

FIG. 7 TRUE TANGENTIAL STRESS — TANGEN
COMPOSITE PR

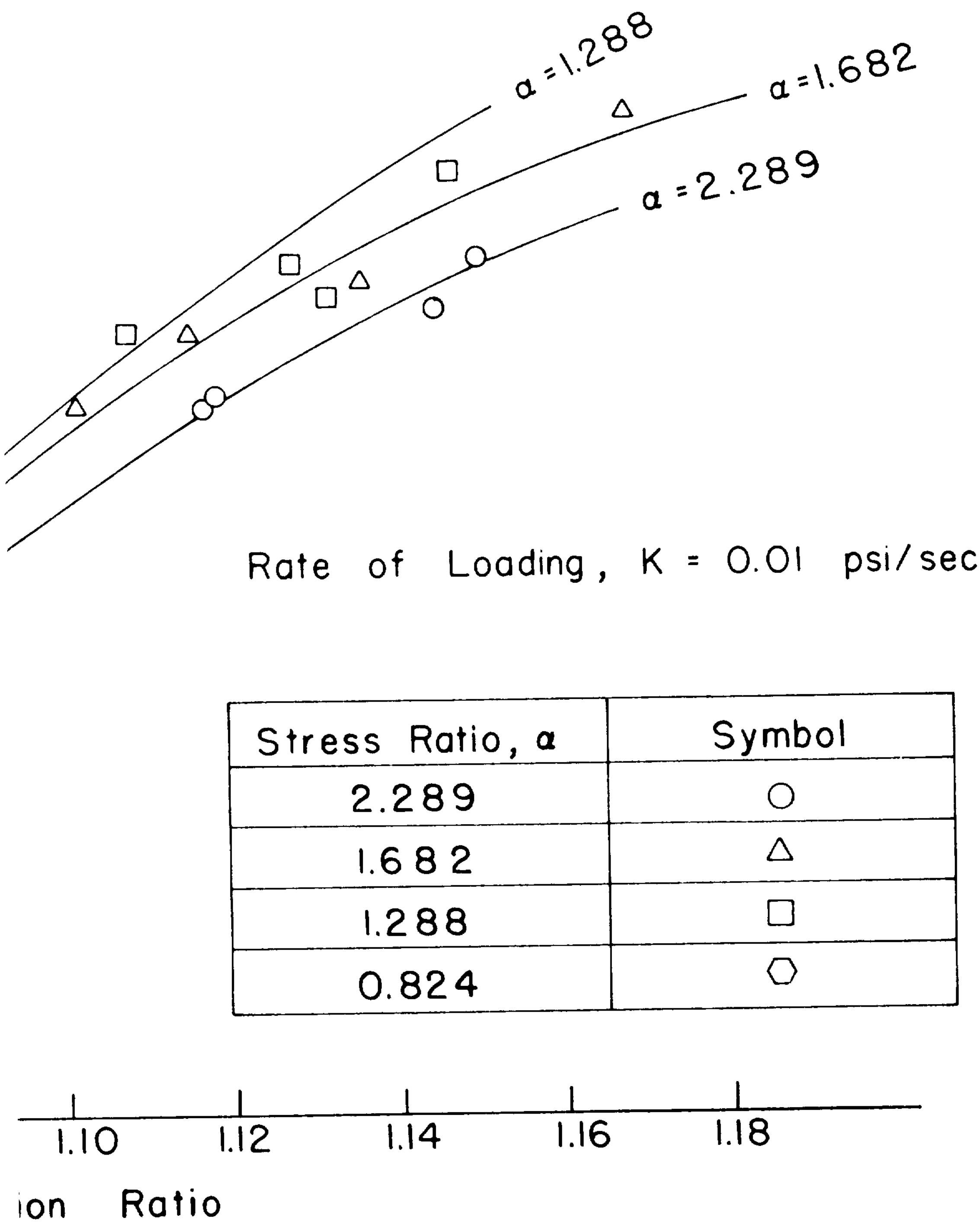

IAL EXTENSION RATIO CURVES FOR THE INERT
ELLANT

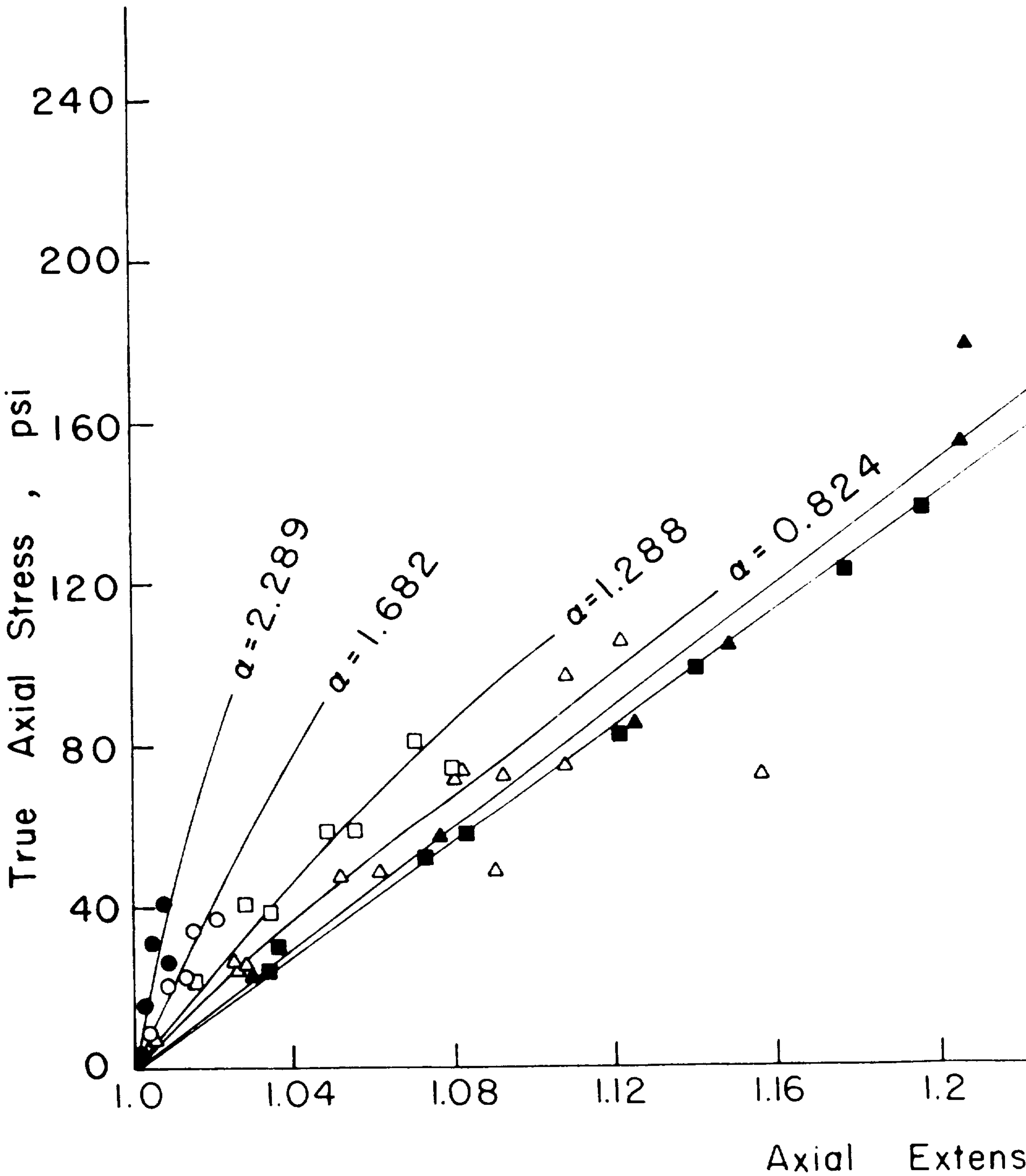

FIG. 8 TRUE AXIAL STRESS — AXIAL EXTEN

PROPELLA

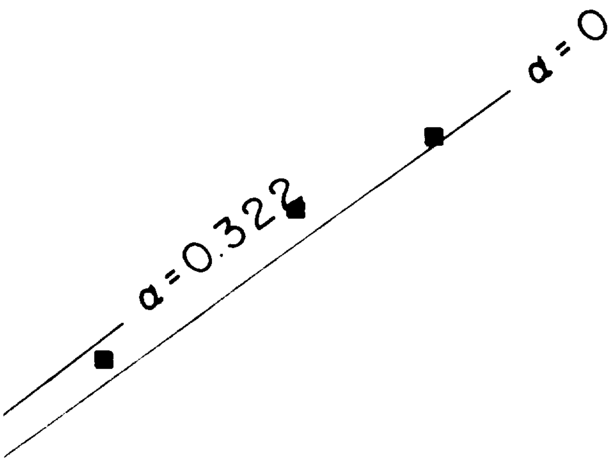

Rate of Loading , K = 10 psi/sec

Stress Ratio , α	Symbol
2.289	●
1.682	○
1.288	□
0.824	△
0.322	▲
0	■

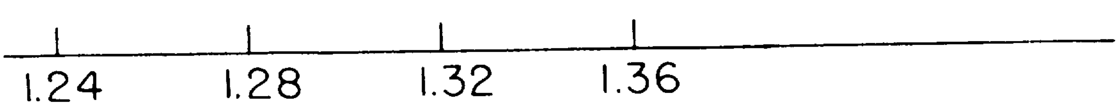

n Ratio

ION RATIO CURVES FOR THE INERT COMPOSITE

r

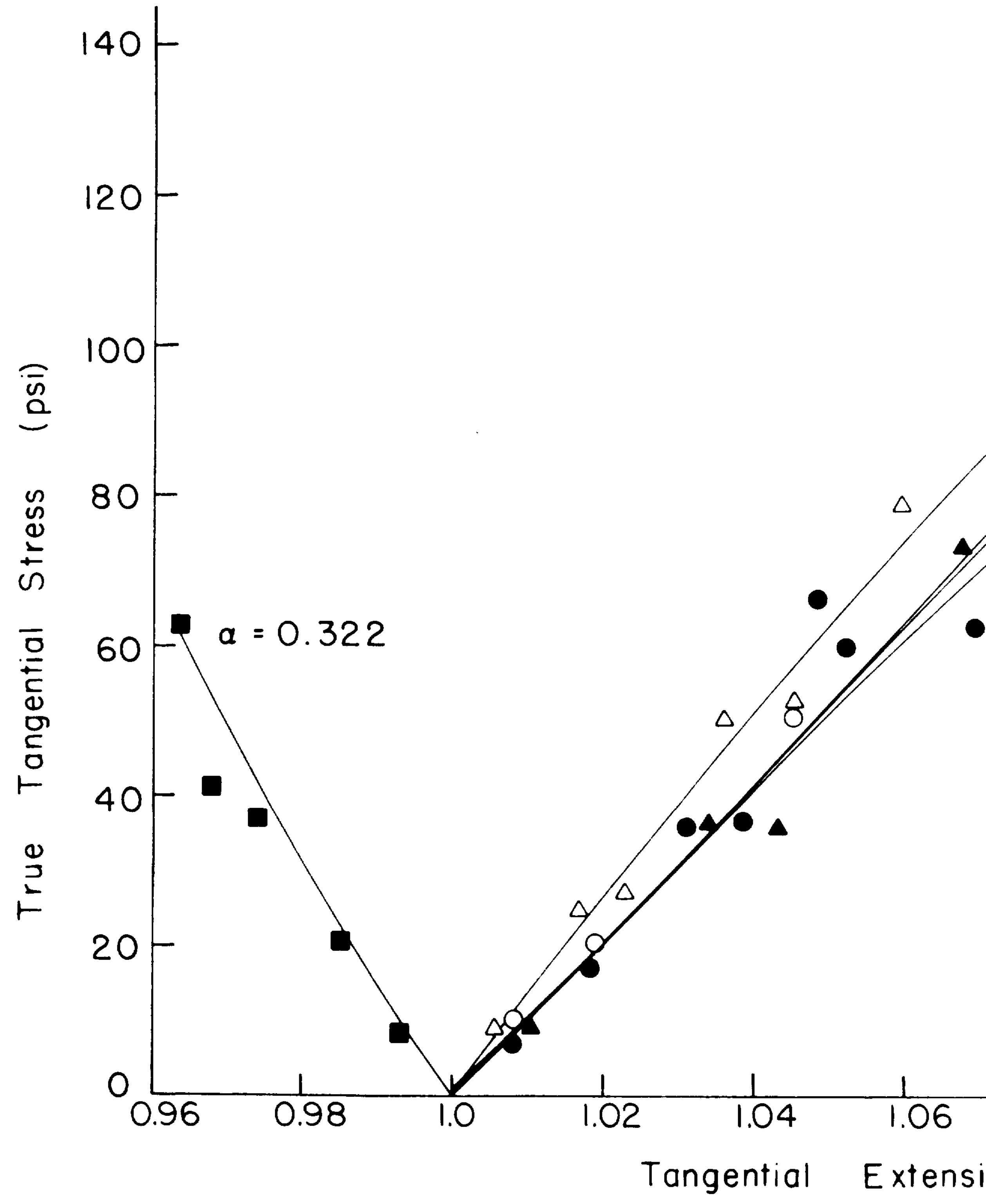

FIG. 9 TRUE TANGENTIAL STRESS — TANGENTIAL
COMPOSITE F

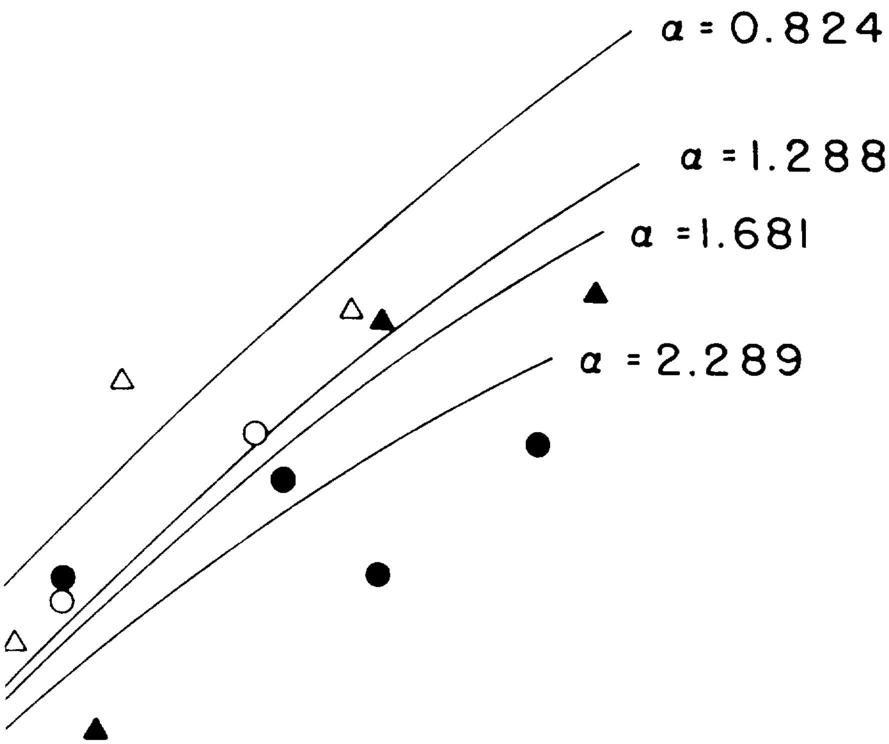

Rate of Loading , K = 10 psi/sec

Stress Ratio, α	Symbols
2.289	●
1.681	○
1.288	▲
0.824	△
0.322	■

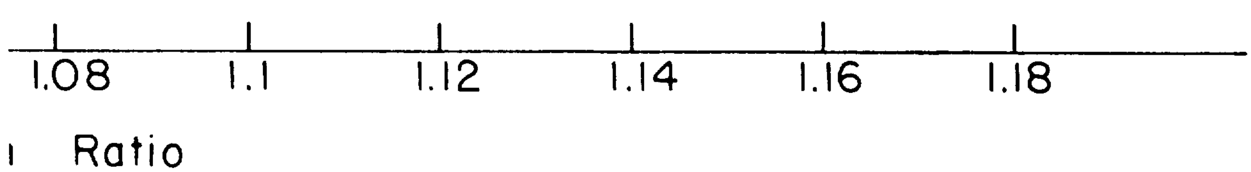

EXTENSION RATIO CURVES FOR THE INERT
OPELLANT

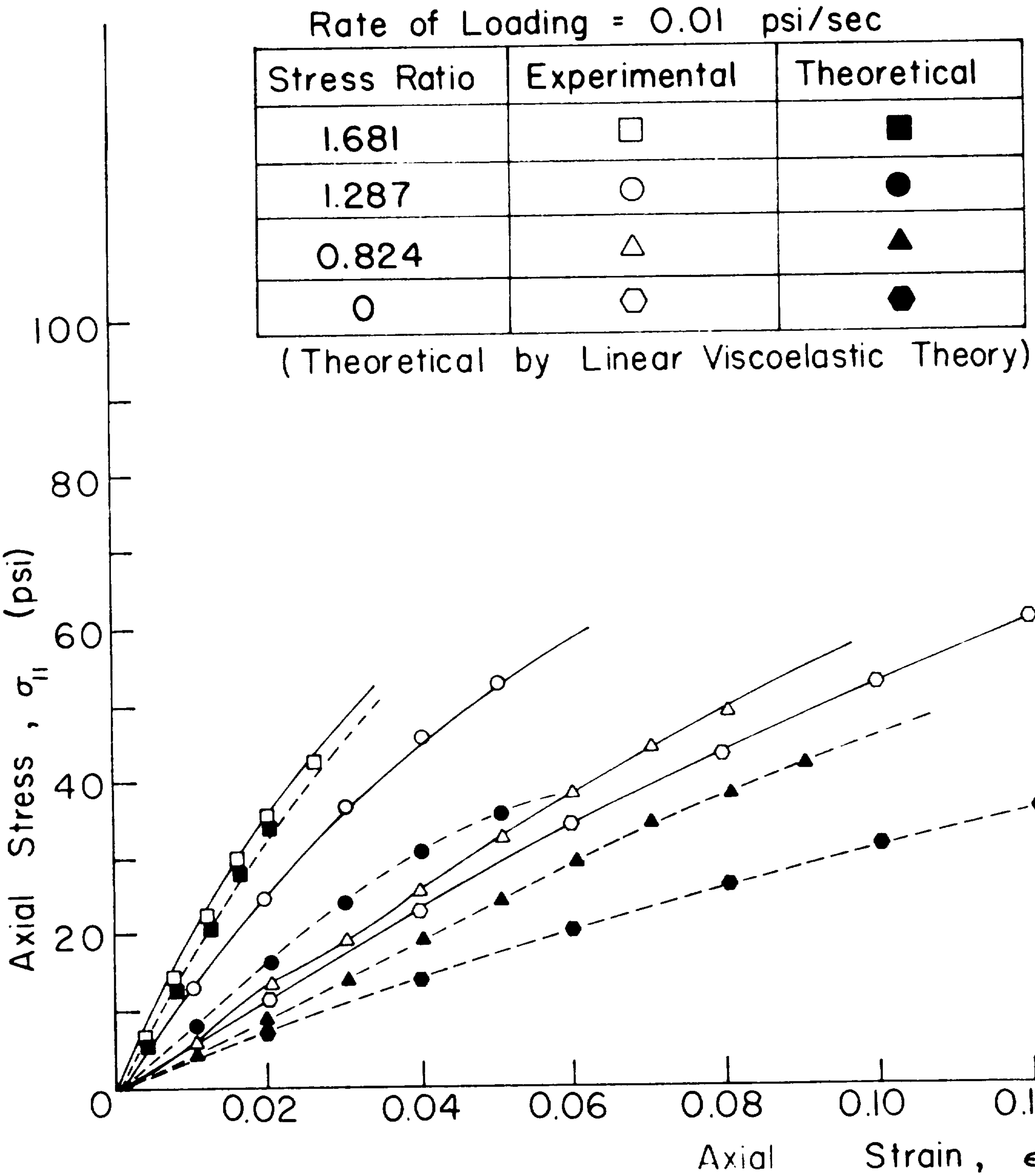

FIG. 10 AXIAL STRESS — STRAIN CURVES FOR T

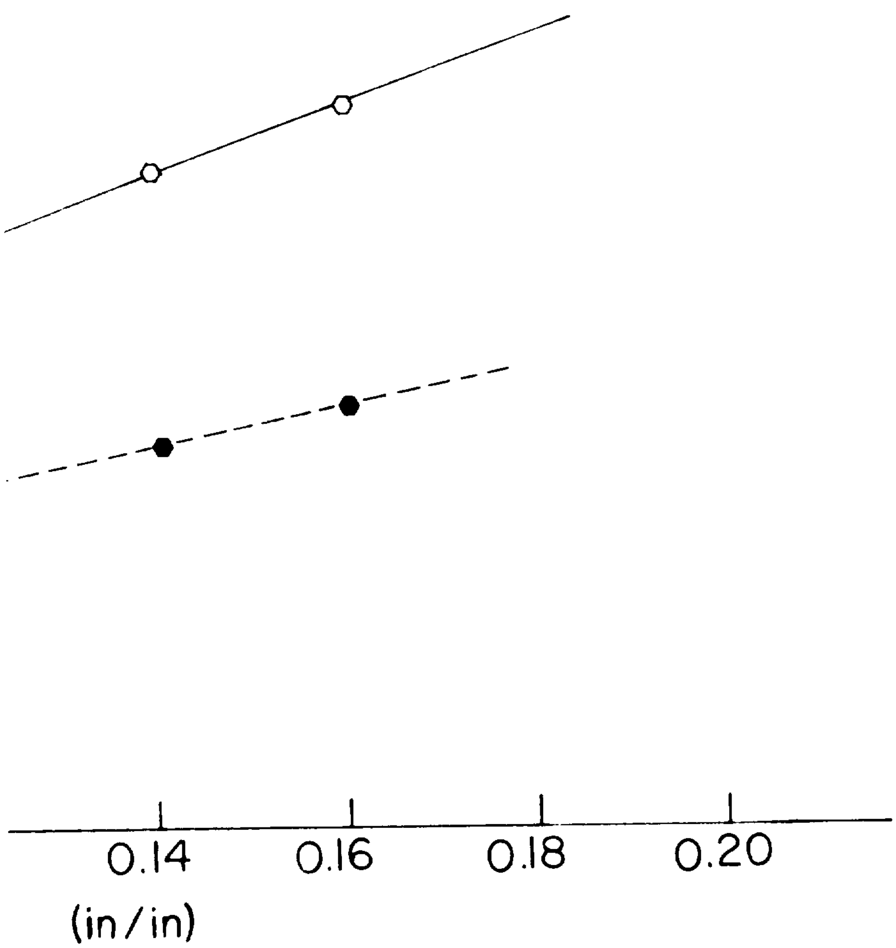

E INERT COMPOSITE PROPELLANT

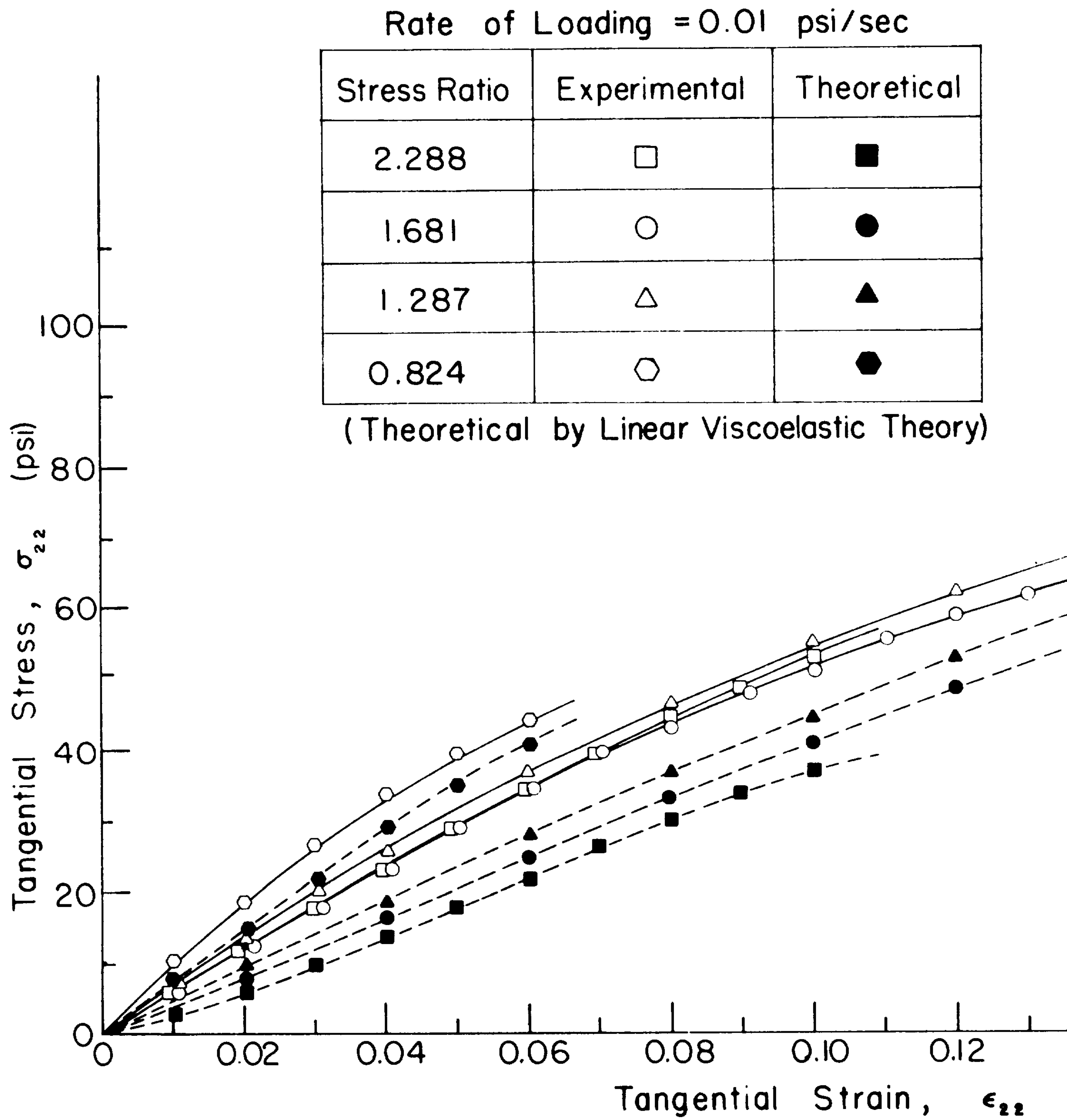

FIG. 11 TANGENTIAL STRESS — STRAIN CURVE

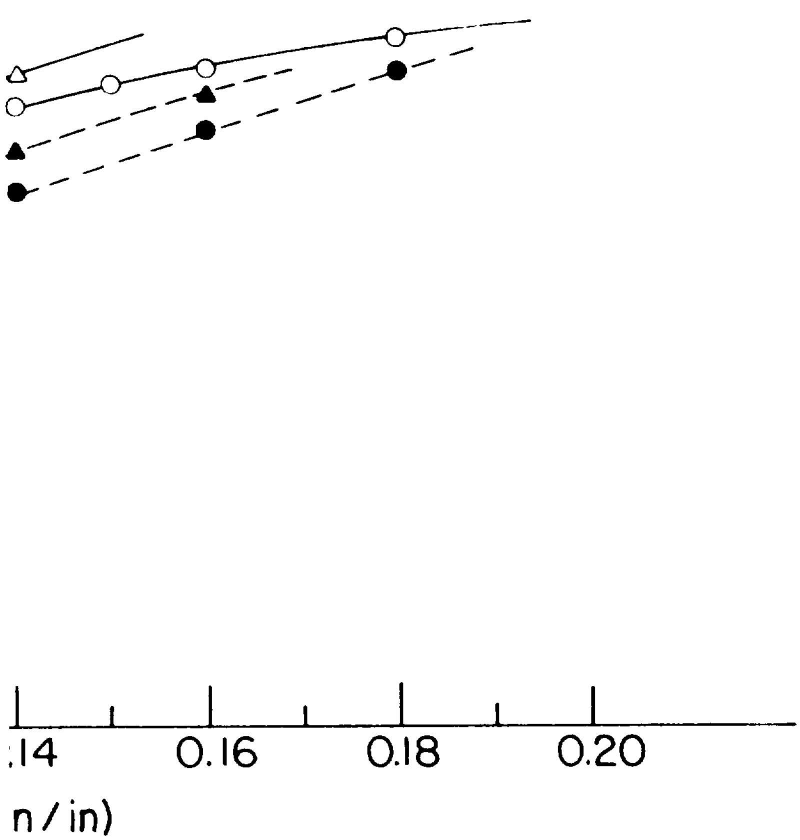

FOR THE INERT COMPOSITE PROPELLANT

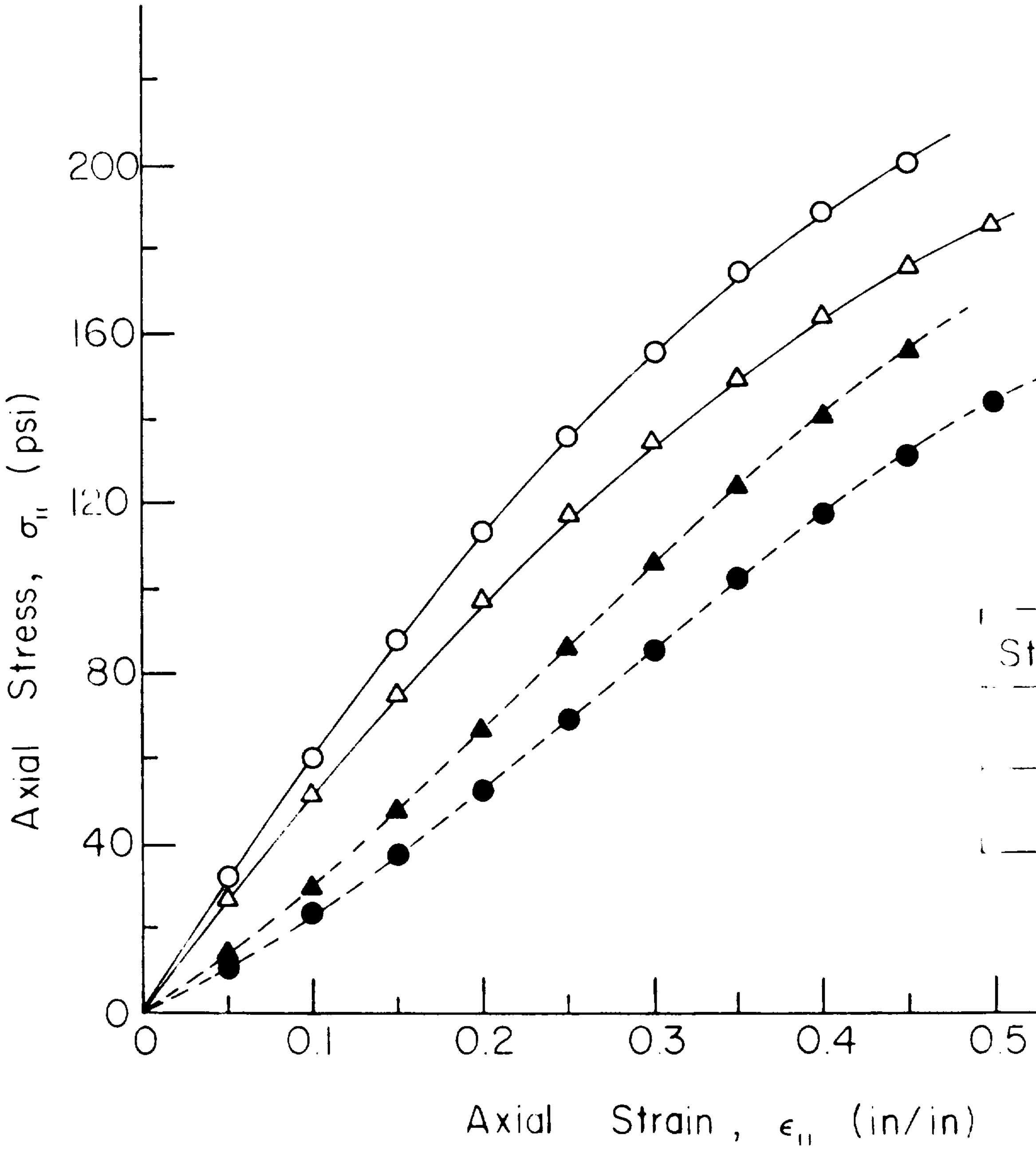

FIG.12 AXIAL STRESS — STRAIN CU

Rate of Loading = 10 psi/sec

ɛss Ratio	Experimental	Theoretical
).322	△	▲
).0	○	●

(Theoretical by Linear Viscoelastic Theory)

ʀVES FOR THE INERT COMPOSITE PROPELLANT

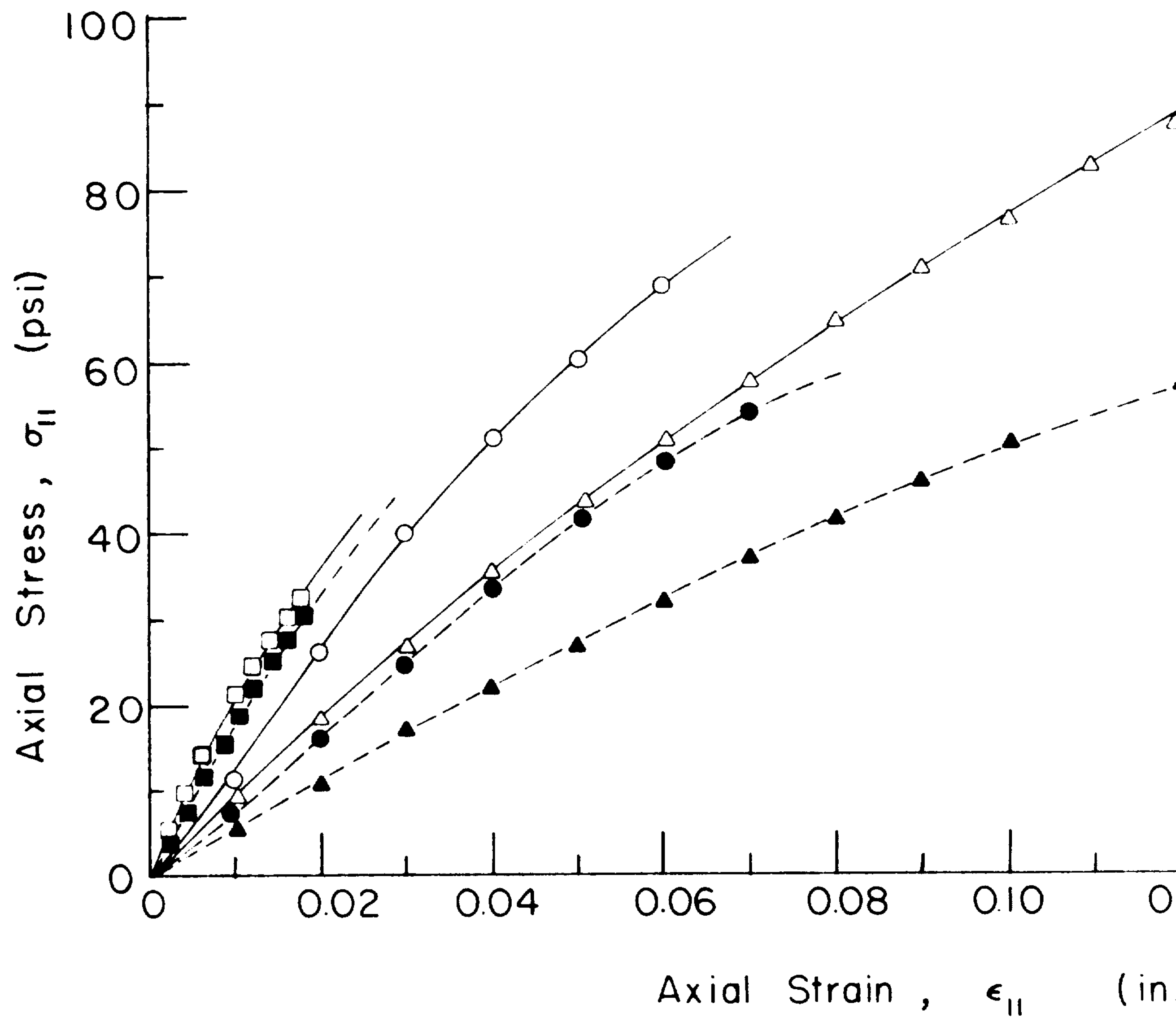

FIG. 13 AXIAL STRESS — STRAIN CURVE

Rate of Loading = 10 psi / sec

Stress Ratio	Experimental	Theoretical
1.681	□	■
1.287	○	●
0.824	△	▲

(Theoretical by Linear Viscoelastic Theory)

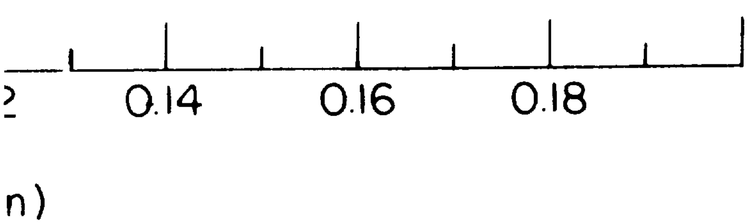

FOR THE INERT COMPOSITE PROPELLANT

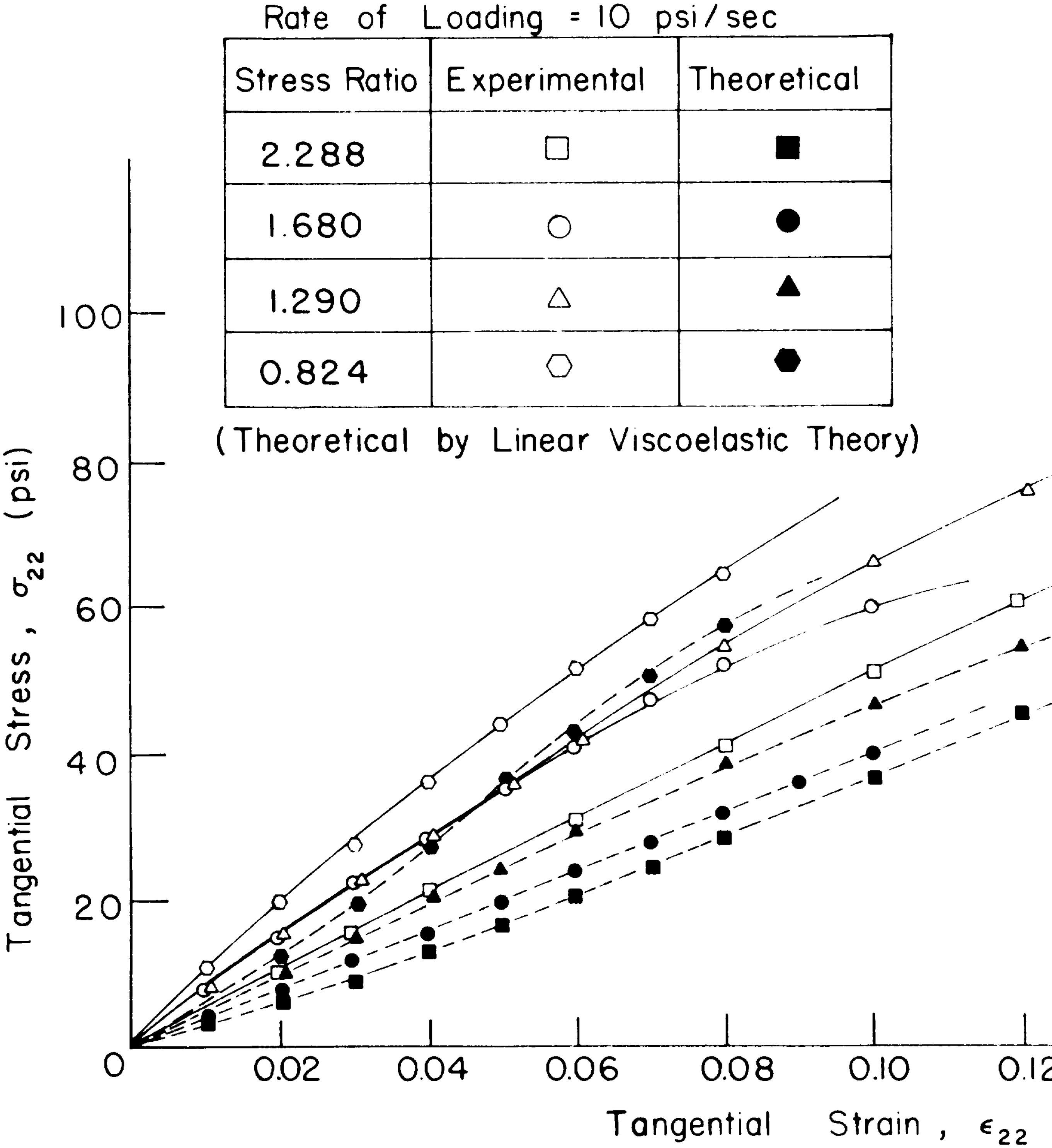

FIG. 14 TANGENTIAL STRESS — STRAIN CURVES F

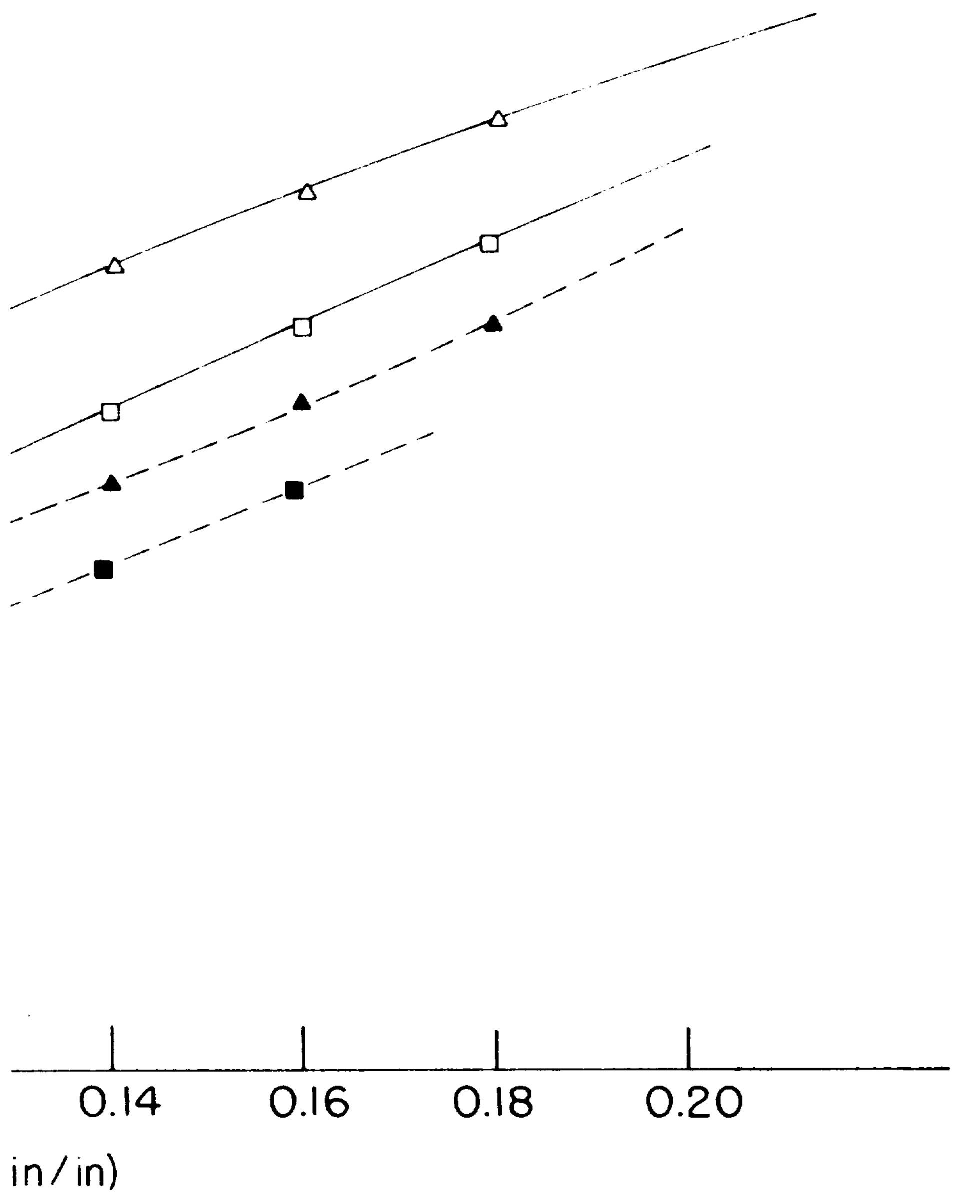

: THE INERT COMPOSITE PROPELLANT

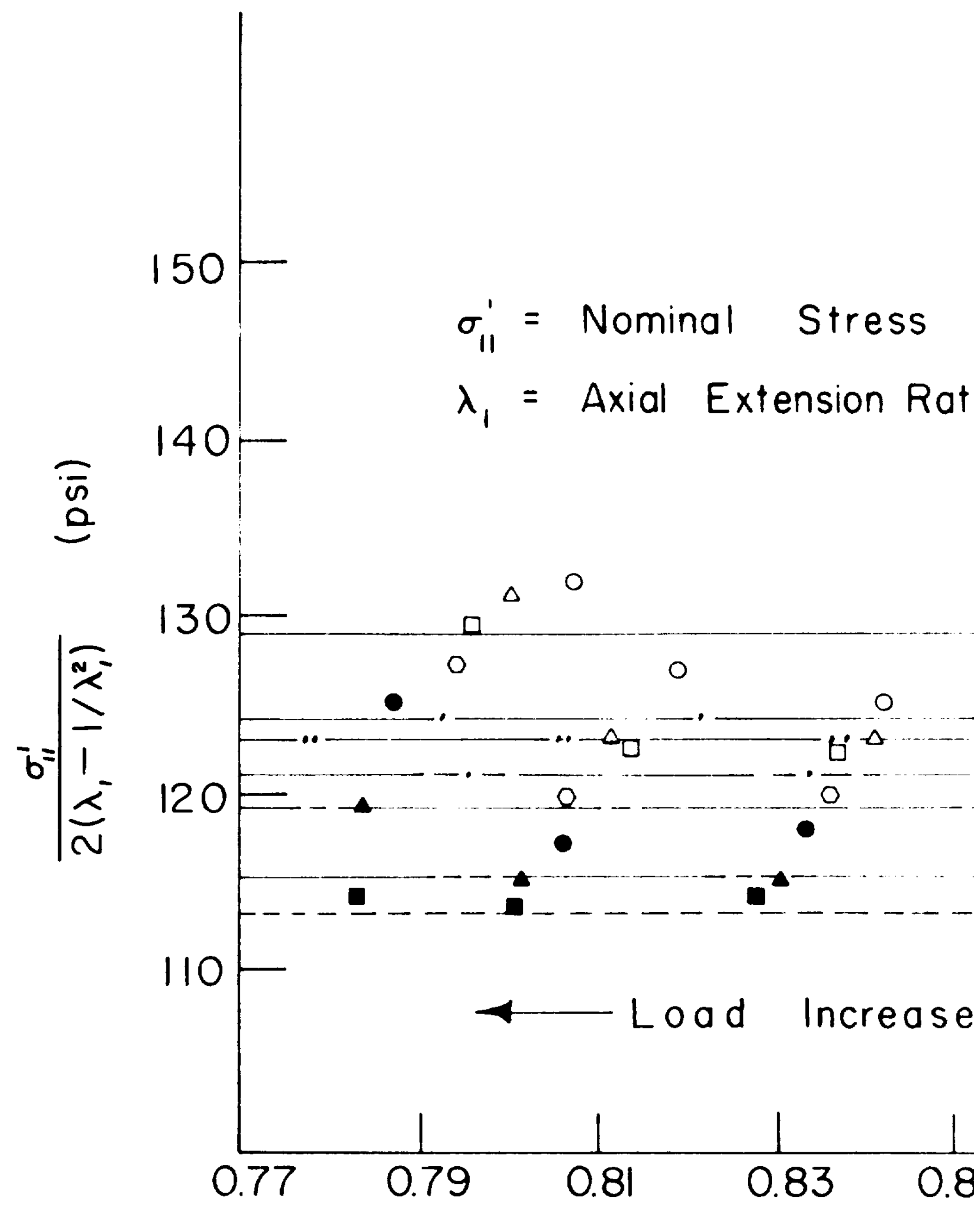

FIG. 15 PLOT OF $\frac{\sigma'_{11}}{2(\lambda_1 - \frac{1}{\lambda_1^2})}$ AGAINST

INERT COMPOSIT

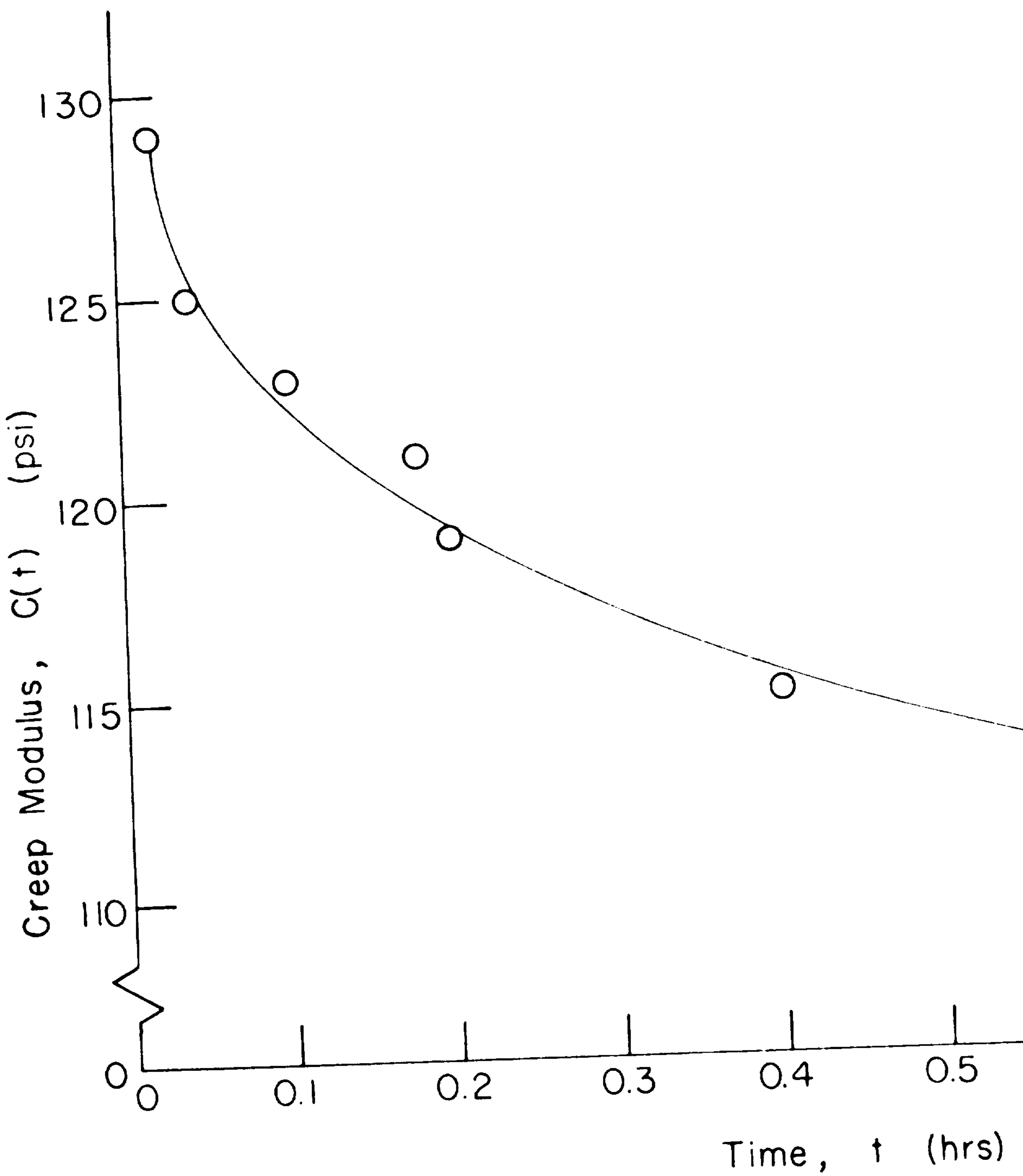

FIG.16 VARIATION OF CREEP MODULUS WITH

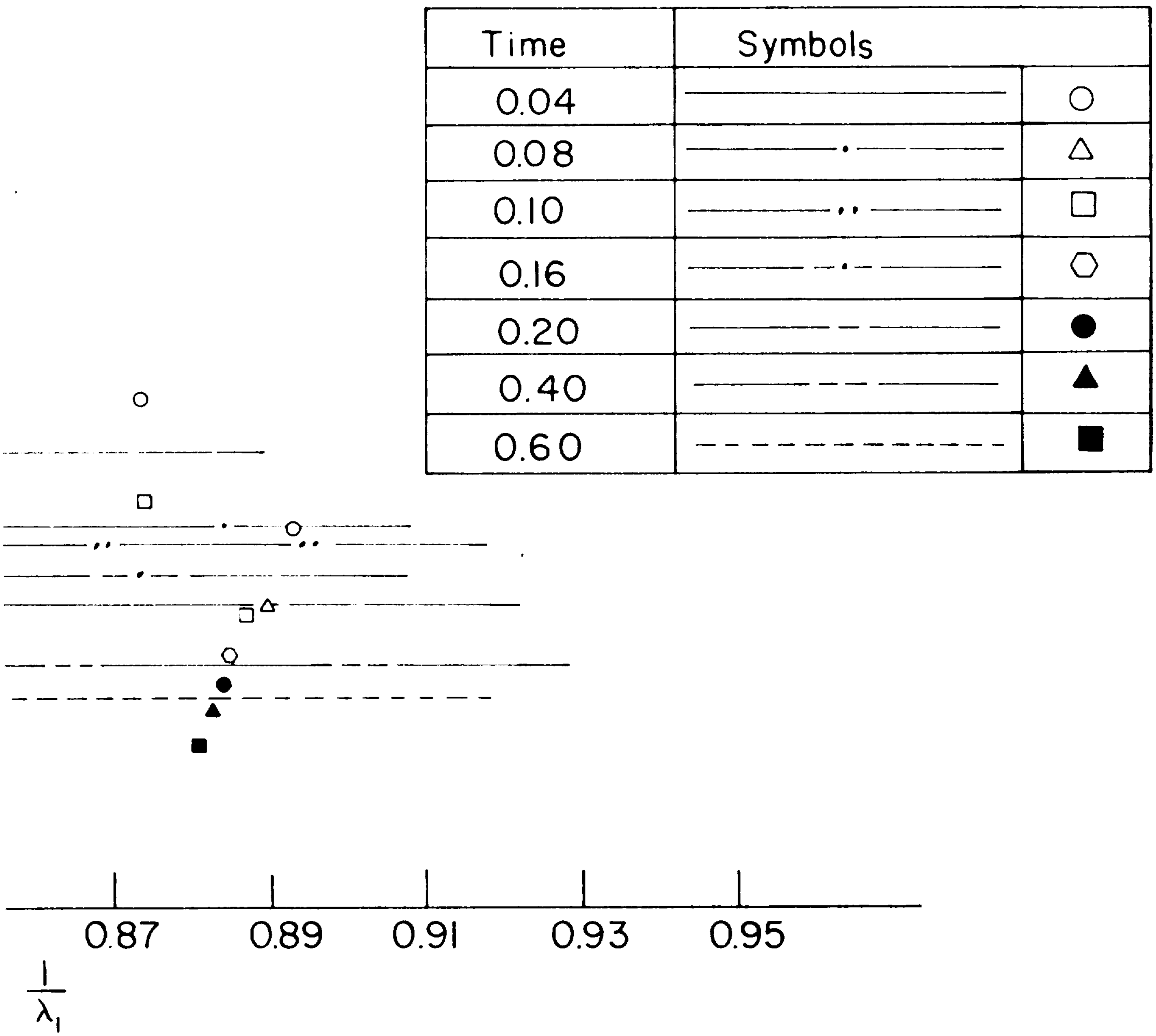

IN UNIAXIAL CREEP EXPERIMENTS FOR THE PROPELLANT

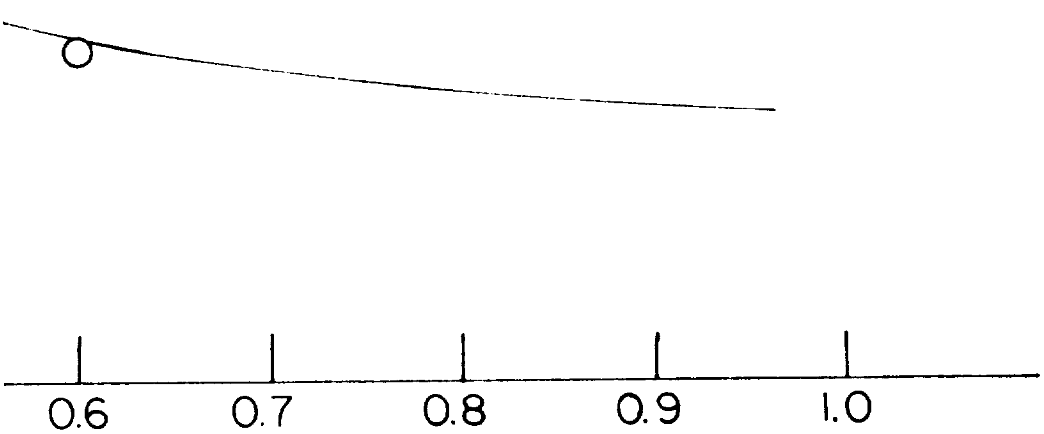

TIME FOR THE INERT COMPOSITE PROPELLANT

SUMMARY OF RESEARCH WORK ACCOMPLISHED UNDER PROJECT ENTITLED "A TEST PROGRAM TO DETERMINE THE MECHANICAL BEHAVIOR OF SOLID FUEL PROPELLANTS" (JPL CONTRACT NO. 950875) DURING THE PERIOD JULY, 1964 to JULY, 1965

Biaxial stress-strain and fracture studies on an inert composite propellant material corresponding to first quadrant of principal stress space were conducted for room temperature conditions. Effect of rate of loading on biaxial stress-strain and fracture behavior was studied. The results on fracture behavior on biaxial loading have been reported in the following reports already submitted to the sponsor.

(1) "The Failure of Polymeric Materials under Biaxial Stress Fields." (Submitted in November, 1964.)

(2) "Failure of an Inert Composite Propellant under Multiaxial Stress Fields." (Submitted in March, 1965.)

Mechanical characterization of an inert composite propellant material for biaxial stress fields corresponding to the first quadrant of principal stress space has been made. The effect of rate of loading on the biaxial stress-strain behavior has been considered. A technical report entitled "Stress-Strain Behavior of an Inert Composite Propellant for Multiaxial Loading Conditions" which covers the results on mechanical characterization is sent herewith.

Biaxial stress-strain and fracture studies on the material under stress fields that corresponded to the second quadrant in the principal stress space were performed. Cylindrical specimens of short lengths (one inch) were used in the studies to prevent buckling. It was found that it was not possible to prevent buckling however short cylindrical specimens were. This study indicated that the technique of producing biaxial stress fields corresponds to the second quadrant by subjecting short cylindrical specimens to combined axial compression load and internal pressure is not suitable. An entirely different technique has been planned to study biaxial stress-strain and fracture behavior in the second quadrant of the principal stress space.

Attempts were made to characterize the test material for multiaxial loading, in terms of a stored energy function ϕ and a dissipated energy function ψ. The experimental data from biaxial hysteresis experiments (triangular stress history) were used for the determination of the above functions ϕ and ψ. The results indicate that some of the material constants in the dissipated energy function become negative as a consequence of strain rate invariants (in terms of principal extension ratio rates) being non-symmetric. The investigator has not been able to give physical interpretation of the above result.

The experimental facility was improved to study biaxial stress-strain and fracture behaviors at elevated and low temperatures. Plans are underway to modify the present experimental facility to study triaxial stress-strain and fracture properties of the material. Specimen preparation method was considerably improved to obtain consistent results in mechanical behavior studies.